Sixth Order Generalized Integrator Based Power Quality Improvement in Renewable Energy Systems

Priyank Nema[1†], Sivasankaran V[2*†], Narendra Babu P[3†]

[1,2*,3]School of Electrical and Electronics Engineering,

VIT Bhopal University, Kotrikalan, Bhopal-Indore Highway, Sehore, 466001, M.P, India.

*Corresponding author(s). E-mail(s): sivasankaran@vitbhopal.ac.in[2],

+91 9843856991;

Contributing authors: priyank.nema2021@vitbhopal.ac.in[1], +91 7999554623;

narendrababu.p@vitbhopal.ac.in[3], +91 6281571216;

[†]These authors contributed equally to this work.

Abstract

A Sixth-Order Generalized Integrator (SiOGI) with a Frequency-Locked Loop (FLL) control system is simulated in this paper. The proposed SiOGI-FLL addresses Power Quality (PQ) challenges by integrating nonlinear loads to remove power quality issues under Direct Current (DC) offset, grid harmonics, and unbalanced grid conditions. The developed SiOGI-FLL tackles power quality problems associated with renewable energy integration with the grid. The SiOGI-FLL system offers enhanced frequency tracking and precise phase detection, which helps maintain accurate synchronization with the grid. The proposed system can efficiently improve PQ issues and ensure seamless integration of Renewable Energy Sources (RESs) by utilising advanced control techniques. To evaluate the performance of the proposed SiOGI-FLL, extensive simulation studies are conducted under various operating conditions, such as DC offset, unbalanced grid, and grid harmonic scenarios with Linear Load (LL), Non-Linear Load (NLL), and UnBalanced Loads (UBL). The simulation results demonstrate the superior capabilities of the SiOGI-FLL control scheme.

Keywords: Sixth Order Generalized Integrator - Frequency Locked Loop (SiOGI-FLL), Renewable Energy Sources (RESs), Power Quality (PQ), DC offset, Grid harmonics, Unbalance grid, Voltage Source Converter (VSC).

1 Introduction

In developing and undeveloped countries, the demand for electrical energy is increasing daily due to industrialization. Conventional sources of electrical power, such as coal, natural gas, etc., are used to meet this load demand due to the lack of traditional energy sources and the reduced effect of the greenhouse effect due to using conventional energy sources. Renewable Energy Sources (RESs), such as solar, fuel cells, wind etc., are also used with non-renewable energy sources. Among the RESs, solar energy is better because sunlight is directly converted into electricity using solar panels, which can be used on rooftops or in grid-connected condition. When the solar panel is connected to a grid, various kinds of power quality problems arise due to the unpredictable nature of sunlight. The Maximum Power Point Tracking (MPPT) controller extracts the peak power from the solar panel, such as Perturb and Observe (P&O). As well, developing and undeveloped countries' grids are often weak, unreliable, and have low electricity quality. A weak grid not only struggles to maintain stable voltage and frequency levels under load variations and disturbances, but it also presents operational challenges. Such grids typically have high impedance and low short-circuit capacity and are susceptible to voltage instability and frequency deviations. In various research articles, a weak grid is defined as a power system with limited capacity to absorb power fluctuations due to its high impedance and low short-circuit power, which leads to voltage instability and operational challenges explained by Suvorov and Aleksey et al. [1]. Direct Current (DC) offset, harmonics, and unbalancing come under the weak grid. As a result, in addition to the usual problems, integrating renewable energy into the grid faces additional challenges. The grid acts as an energy buffer in a grid-connected system, and renewable energy-generated power can be sent into the grid. However, due to nonlinear or unpredictable demand, the grid voltage can suffer from Power Quality (PQ) issues such as voltage sag and swell, over and under voltages, very short interruption, voltage spike, voltage fluctuation, voltage unbalance, DC offset, harmonics, and so on. As a result, feeding renewable energy into the grid becomes challenging in this situation given by Jha and Shaik [2]. Furthermore, in the case of microgrids, these difficulties are more prominent since unanticipated load changes, such as UnBalanced Loads (UBL), Non-Linear Loads (NLL), any fault condition, and so on, are translated into grid voltage distortion, frequency variations, and so on described by Kumar and Prabakaran et al. [3].

The Voltage Source Converter (VSC) serves as a grid-supporting converter, helping to feed RESs explained by Badoni and Singh et al. [4] electricity into the grid successfully and reducing PQ issues during renewable energy integration. It can also be used to reduce harmonics and raise the power factor shown by Xue and Ding et al. [5] with the proper control. The related work section describes various controllers used to control VSC. In this paper, a SiOGI-FLL is proposed with extreme harmonics and DC offset reduction capability. Whereas the other controller was unable to remove the excessive DC offset component from the grid, the settling time was lowered as compared to the other controller. In this work, MATLAB simulation software is employed, and simulations are performed under an unbalanced grid, grid voltage with DC offset, polluted grid conditions, and Fast Fourier Transform (FFT) analysis is also done. All of the controller's internal results are displayed at the same time. The following are the distinguishing features of the proposed control scheme.

I. The proposed SiOGI-FLL control method draws the Fundamental Component (FC) from the load currents and Positive Sequence Components (PSCs) from the grid voltages.
II. The amplitude, frequency, and phase angle can all be adaptively evaluated using the suggested control method.
III. The proposed controller is stable and has good dynamic and steady state response with no overshoot and less settling time.
IV. The proposed controller is capable of eliminating the lower and higher-order harmonics present in the polluted grid voltages and currents.
V. The proposed controller is capable of eliminating grid harmonics and DC components from the grid and converting an unbalanced grid into a balanced grid.
VI. The renewable system's feed-forward component is integrated into the control framework to enhance the system's dynamic behaviour.
VII. The proposed control method matches the recently proposed control scheme. So, it is justified that the proposed controller performance is better than all other control techniques for power quality enhancement and clean power conversion.

This work is separated into eight sections, the first section describes the introduction. Section two describes the related work, section three describes the system model description, section four explains the control strategy. Section five discusses the proposed controller's stability analysis. Section six describes the outcome and provides a detailed explanation of all simulated results. Section seven compares the proposed controller with other recently developed controllers. Section eight discusses the conclusion. Additionally, a table of abbreviations and their full forms has been created in Table 1, listing all abbreviations, variables, and symbols used in this research paper.

2 Related Work

To control VSC, various conventional and adaptive control algorithms are proposed, including Instantaneous Reactive Power Theory (IRPT) explained by Tuyen and Fujita [6], Synchronous Reference Frame (SRF) explained by Lakshmanan and Rajpurohit et al [7], fryze current compensation theory-based controller explained by Latha and Sujatha et al. [8], ADAptive LInear NEuron (ADALINE) implemented by Chawda and Shaik [9], Neural Network (NN)-based controller explained by Srikanth and Kumar [10], Kalman Filter (KF)-based controller implemented by Çelik and Ahmed et al. [11], Wavelet Transform (WT)-based controller implemented by Pattanaik and Swain et al. [12], and Discrete Fourier Transform (DFT)-based controller implemented by Priyadarshini and Krishna et al. [13]. The IRPT theory cannot produce satisfactory outcomes in unbalanced and distorted situations. The SRF theory-based controller also performs poorly under various dynamic load conditions because of the low-pass filter. Although the fryze and ADALINE techniques perform well in steady-state and dynamic situations, they perform poorly in distorted grid conditions. The NN techniques suffer from improper learning during system frequency changes. Under grid transient situations, KF-based controllers, WT-based controllers, and DFT-based controllers all fail to improve system dynamic performance described in references [6–13]. Furthermore, numerous adaptive control systems have been investigated in recent years, including least mean square implemented by Kumar and Kumar [14], least mean fourth implemented by Alam and Arya [15], normalized least mean fourth implemented by Dey and Subudhi [16], recursive least square implemented by Somalwar and Kadwane et al. [17], variable step size least mean square implemented by Jalal and Yang et al. [18], improved linear sinusoidal implemented by tracer Singh and Jain et al. [19], and adaptive notch filter implemented by Somkun and Srita et al. [20]. However, they have several limitations, such as insufficient pursuit of the steady-state response due to higher order optimization, increased complexity, high computing cost, and poor weight convergence rate described in references [14 – 20]. However, in terms of grid synchronization and DC offset rejection, the aforementioned controllers are not the best. A few Generalized Integrator (GI)-based control systems have recently been published in the literature to solve the issues raised above. Power converter control has been using GI-based control techniques for the past 20 years. Building a Proportional-Resonant (PR) controller for fixed-frame current regulation is the most well-known use of GI explained by Althobaiti and Ullah et al. [21]. Aside from the PR controller, another significant use is the construction of the Quadrature Signal Generator (QSG), with the resulting structure known as a Second-Order GI-based QSG (SOGI-QSG) shown by Xu and Qian et.al. [22]. To acquire all of this information and synchronise the RESs with the grid, a SOGI controller is used, which can be used for grid synchronization as a Phase-Locked Loop (PLL) and frequency estimation as a FLL analysed by Golestan and Guerrero et al. [23]. Because the design of a PLL uses a SRF, it is more complex than that of a FLL. Hence, the FLL structure is typically employed. The SOGI controller does not have the capability to eliminate harmonics and PQ arising due to DC offset, which has a negative impact on system performance concluded by Narayanan and Singh [24]. To address these concerns, a third-order generalised integrator is developed, which has been shown to have a superior filtering characteristic than the SOGI. It is also known as an Improved SOGI (ISOGI)-based algorithm in some publications. The ISOGI can reject both lower-order and higher-order harmonic components and has a low-magnitude DC offset, as evidenced by a frequency domain plot (bode plot). The described ISOGI-based control method is more stable and versatile than standard algorithms and has excellent filtering capabilities. However, its design specifications are not specified. The parameters utilised are based on experience, which is unreliable explained and concluded by Shah and Hussain et al. [25]. For reducing system complexity, some researchers introduce a Reduced Order Generalized Integrator (ROGI) and a Modified ROGI (MROGI)-based controller implemented by Babu and Guerrero et al. [26]. Another controller for reducing SOGI limitations is the notch filter-based controller. In the notch filter controller, an additional notch filter branch is added to eliminate the effect of DC offset in the conventional SOGI controller, as a result of which some new parameters are introduced in the traditional SOGI controller, and at the same time, the parameter selection in the SOGI controller gets tough analysed by Jain and Singh [27]. To solve the problem of DC offset, a Mixed Second Third Order Generalized Integrator (MSTOGI) is used, in which an additional branch is added, which reduces the effect of DC offset in the input signal implemented by Zhang and Zhao et al. [28]. The MSTOGI can precisely lock the phase in non-ideal grid voltage scenarios like imbalance, including DC offsets and harmonics, without adding any further parameters analysed by Chakraborty and Modi et al. [29]. Another technique that uses extra SOGI as prefilters and has outstanding filtering characteristics for both low- and high-frequency components was developed. Furthermore, for simplicity, the damping factors for each SOGI were assumed to have the same value, which could be more logical and may limit the method’s efficacy observed by Naqvi and Singh [30]. Two SOGI blocks are connected in series to generate a Cascade SOGI (CSOGI), which can remove the dc offset from the input signal. The CSOGI is less difficult to install because the CSOGI's transfer functions are fourth-order functions explained and implemented by Modi and Singh [31]. To address all of the shortcomings in the literature, a Second Order - SOGI (SO-SOGI) was presented, which has improved low- and high-frequency attenuation performance. An entire parameter design process is also accessible in the literature. Its parameters are chosen based on the system's settling time. Which works by converting the fourth-order system into the lower-order system. By using this approximation, the expected and actual settling times differ from each other implemented and observed by Mondal and Karuppaswamy [32]. A cascaded structure with non-identical parameters for the individual is implemented to address this limitation, known Cascaded Non-Identical SOGI (CNISOGI). Compared to SOSOGI, CNISOGI provides greater latitude for faster settling times implemented and explained by Narayanan and Singh [33]. All of these controllers belong to the fourth order. Furthermore, a unique parameter selection approach is created that accurately forecasts the overall settling time of the cascaded system. The dominating closed-loop pole technique is traditionally employed to analyse higher-order strategies explained in Ogata [34]. Some researchers make Multilayer SOGI (MSOGI) based controllers, which have better harmonic elimination capability. After that, they create a Fifth-Order Generalized Integrator (FOGI) controller. FOGI's filtering effectiveness is exceptional since it is specifically built to filter out all aberrant grid voltage circumstances. All GI-based controllers can be utilised in two ways: first, to extract positive and negative sequence components, and second, as a multi-layer to eliminate specific harmonics implemented by Babu and Peesapati et al. [35]. In order to overcome the above limitation, in this paper, a SiOGI-FLL controller is proposed.

3 System Model Description

Figure 1 describes the complete system model in which RESs are connected to the power grid. RESs, such as solar Photovoltaic (PV) through the DC-DC converter and DC-AC inverter are connected. A (P&O)-based MPPT controller has been used to receive peak power from RESs, and the boost output is connected to the VSC capacitor. The Proportional and Integral (PI) controller is used to compute. An interfacing inductor is used to connect the VSC to the grid. The proposed SiOGI-FLL controller mitigates all types of power quality problems arising from various weak grid conditions connected to NLL and UBL. In this paper, a grid-tied system is developed that is coupled to a linear RL load and an unregulated rectifier that operates as an NLL.

3.1 Calculation of DC Link Voltage

The value of the DC link voltage can be obtained from the following equation: For proper operation of the VSC, the value of the DC link voltage should be more than twice the per-phase grid voltage.

$$V_{dc} = \frac{2\sqrt{2}V_{LL}}{\sqrt{3}m} \tag{1}$$

V_{LL} represents the grid line voltage, V_{dc} represents the DC link voltage, and m represents the modulation index.

For finding V_{dc}, put $V_{LL} = 230$ Volt and $m = 1$

$$V_{dc} = \frac{2 * \sqrt{2} * 230}{\sqrt{3} * 1} \tag{2}$$

$$V_{dc} = 375\,Volt \tag{3}$$

For proper operation of VSC, the value of the DC link voltage should be 375 volts, which comes while considering $m = 1$, which is the critical modulation condition.

4 Proposed Adaptive Control Method

Figures 2 and 3 represent the proposed complete adaptive control scheme. To eliminate all types of power quality problems arising from weak grids, NLL and UBL, anti-harmonic current is needed, which is obtained through compensation current. To achieve the compensation current, the following steps are required:

I. Convert the three-phase grid voltage and load current into αβ components using the Clarke transformation.
II. Transform the $\alpha\beta$ components of the grid voltage and load current into in-phase and quadrature components using the proposed SiOGI-FLL controller.

III. Calculate the positive sequence $\alpha\beta$ components of the grid voltage and load current using these in-phase and quadrature components.

IV. Convert these positive sequence $\alpha\beta$ components back into the three-phase positive sequence grid voltage and current using the inverse Clarke transformation.

V. Calculate the positive sequence in-phase and quadrature voltage Unit Vector Templates (UVT) and determine the magnitude of the positive sequence grid voltage using the three-phase positive sequence voltage components.

VI. Compute the active power component of the load current using sampling-hold and absolute circuits, then calculate the average active power component of the load current.

VII. Determine the total or net current using the average active power component of the load current, loss component current, and renewable feedforward current.

VIII. Calculate the compensation current using the in-phase positive sequence UVT and the net current.

IX. Finally, use a hysteresis controller to calculate the firing signal for the VSC, which can generate the anti-harmonic current to mitigate all power quality problems.

The detailed explanation of control stagettes is discussed in the further sub-section.

4.1 Modelling of Proposed Controller and QSG Stage:

Figure 3 shows the proposed SiOGI-FLL. The proposed controller comprises three SOGIs whose parameters are non-identical and are used to generate direct axis (V') and quadrature axis signals (qV'). $G_1(s)$ and $H_1(s)$ represent the transfer functions that link the outputs V' and qV' to the input V, respectively.

$$\begin{aligned} G_1(s) &= \left(\frac{K_1\omega' s}{s^2 + K_1\omega' s + \omega'^2}\right)\left(\frac{K_2\omega' s}{s^2 + K_2\omega' s + \omega'^2}\right)\left(\frac{K_3\omega' s}{s^2 + K_3\omega' s + \omega'^2}\right) \\ H_1(s) &= \left(\frac{K_1\omega' s}{s^2 + K_1\omega' s + \omega'^2}\right)\left(\frac{K_2\omega' s}{s^2 + K_2\omega' s + \omega'^2}\right)\left(\frac{K_3\omega'^2}{s^2 + K_3\omega' s + \omega'^2}\right) \end{aligned} \tag{4}$$

SiOGI-FLL transfer functions equations 4 are sixth-order band-pass filters with corner frequency as ω' rad/s. The damping factors ξ_1, ξ_2 and ξ_3 of the transfer functions equation 4 are related to K_1, K_2 and K_3, as $K_1 = 2\xi_1$, $K_2 = 2\xi_2$ and $K_3 = 2\xi_3$ are different for SOGI-1 and SOGI-2. SOGI-3. The proposed SiOGI has excellent band pass filter characteristics to solve grid harmonics, DC offset, and unbalanced grid problems. However, the proper selection of K_1, K_2, K_3 and λ is required; for the values $K_1 = 1.452$, $K_2 = 1.6$, $K_3 = 2$, and $\lambda = -1$, the system is stable. The characteristic equation of the proposed controller is given in equation 5.

$$\phi(s) = s^6 + (K_1 + K_2 + K_3)\omega' s^5 + (K_1K_2 + K_2K_3 + K_3K_1 + 3)\omega'^2 s^4 + \\ (2K_1 + 2K_2 + 2K_3 + K_1K_2K_3)\omega'^3 s^3 + (K_1K_2 + K_2K_3 + K_3K_1 + 3)\omega'^4 s^2 + (K_1 + K_2 + K_3)\omega'^5 s + \omega'^6 \tag{5}$$

Where ω' is the corner frequency of the controller and K_1, K_2 and K_3 are the gains of the controller.

4.1.1 Parameter Selection for SiOGI-FLL

The objective of the parameter selection technique is to minimise the settling time of the SiOGI-FLL. The system's settling time, based on its parameters K_1, K_2 and K_3, is sought to allow for tuning during the design process to achieve the shortest possible settling time.

4.1.1.1 Selection Process for K_1, K_2 and K_3

The parameters K_1, K_2 and K_3 depend on the damping coefficients ξ_1, ξ_2 and ξ_3. Changing the values of ξ_1, ξ_2 and ξ_3 changes the system's stability and settling time. Firstly, the value of ξ_3 was set to 1, which makes SOGI-3 critical damping, and the other two damping factors were underdamped, whose values lie between 0 and 1. Now, the system's settling time was obtained with the help of MATLAB software at different values of ξ_1 and ξ_2, and the values at which the minimum settling time was obtained were considered the final values of ξ_1 and ξ_2. Finally, $\xi_1 = 0.726$ and $\xi_2 = 0.8$. The lowest settling time is obtained at $\xi_1 = 0.726$, $\xi_2 = 0.8$, and $\xi_3 = 1$, and the system is also stable, and $K_1 = 1.452$, $K_2 = 1.6$ and $K_3 = 2$ are calculated with the help of ξ_1, ξ_2 and ξ_3.

Figure 4 shows a flowchart that explains the selection process of K_1, K_2 and K_3. Firstly, take two different values of ξ_1, ξ_2 and ξ_3. Next, determine the values of K_1, K_2 and K_3. Next, determine the settling times, t_{s1} and t_{s2}, using the transfer function of the proposed controller. Next, store the minimum settling time between the two settling times in a new variable, t_{sm}. Next, select new values for ξ_1, ξ_2 and ξ_3. Once again, calculate the settling time using

MATLAB software and store it in t_{sn}. Next, compare the minimum settling time to the newly determined settling time. Next, repeat the same steps by varying the values of ξ_1, ξ_2 and ξ_3 until the minimum settling time is obtained. The final controller gain will be the one that achieves this minimum settling time.

4.1.1.2 Selection Process for λ

The FLL is a highly efficient technique for adjusting the centre frequency of the SiOGI. Figure 3 displays the adaptive filter, which includes the FLL. To comprehend the behaviour of the FLL, it's necessary to analyse the link between the quadrature output signal qV' and the error signal ε_v. Hence, the frequency error variable ε_f can be defined as multiplying qV' and ε_v. The mean value of ε_f will be positive when ω is less than ω', zero when ω is equal to ω', and negative when ω is greater than ω'. Therefore, as depicted in Figure 3, an integral controller with a negative gain $\lambda = -1$ can be employed to nullify the DC component of the frequency error by adjusting the resonance frequency ω' of the SiOGI until it aligns with the input frequency ω.

4.1.1.3 Performance of Controller Under Different Value of Controller Gain

The step response of the proposed controller is calculated at different values of controller gain to demonstrate its robustness, which is shown in Figure 5. The settling time of the system is at its minimum when $K_1 = 1.452$, $K_2 = 1.6$, and $K_3 = 2$.

4.1.2 DC offset Production and Elimination

DC offset in the electrical grid, a remarkably intricate phenomenon, involves a small DC voltage component that is superimposed on the AC voltage of the grid. This complexity can lead to a myriad of issues in the power system, including transformer saturation, increased losses, and the maloperation of protective devices. The areas where DC offset can occur and have an impact are as follows:

4.1.2.1 Transmission Lines

DC offset can be introduced in transmission lines due to GeoMagnetic Disturbances (GMD) caused by solar storms, which induce quasi-DC currents. This is particularly relevant in regions closer to the poles, where geomagnetic activity is more robust. For instance, in [specific incident], a solar storm induced a significant DC offset in the transmission lines of [specific region], leading to [specific consequences].

4.1.2.2 Urban Areas with High Industrial Activity

DC offset can also be caused by industrial equipment such as High Voltage Direct Current (HVDC) systems, large rectifiers, or other power electronic devices that inject DC components into the grid. For instance, a large rectifier used in a steel mill can introduce a significant DC offset into the grid.

4.1.2.3 Areas with Grounding Issues

Poor grounding practices or faults in the grounding system can introduce DC currents into the grid. This is more likely in older infrastructure or areas where the grounding system has been compromised.

4.1.2.4 Regions with High Solar Activity

Areas more susceptible to solar activity, which can induce GMDs, are more prone to experiencing DC offsets. This includes regions at higher latitudes.

4.1.3.5 Proximity to HVDC Converter Stations

Areas close to HVDC converter stations may experience DC offset due to the nature of these systems. HVDC systems convert AC to DC and back to AC, and any imperfections in this process can lead to DC components being introduced into the AC grid.

4.1.2.6 Faulty Equipment or Asymmetrical Loads

Faulty electrical equipment or unbalanced loads in any region can cause DC offsets. This can occur in any part of the grid where such conditions exist.

4.1.2.7 DC Offset Elimination through SiOGI-FLL

DC offsets, a potential threat to the power system, are vigilantly monitored and controlled to prevent damage to the power system components, ensuring reliable operation. The mechanism for eliminating the DC offset from the grid voltage is explained through the following equation:

Assume grid voltage with DC offset.

$$v(t) = V_{dcoff} + V_m \sin \omega t \tag{6}$$

V_{dcoff} represents the DC component present in the grid voltage, V_m represents the amplitude of the grid voltage, and ω represents its supply angular frequency. Now, taking the Laplace transform of the equation.

$$V(s) = \frac{V_{dcoff}}{s} + V_m\left(\frac{\omega}{s^2 + \omega^2}\right) \tag{7}$$

From the proposed SiOGI controller, the direct and quadratic axis transfer functions are

$$\frac{V'(s)}{V(s)} = G_1(s) = \frac{K_1 K_2 K_3 \omega'^3 s^3}{\phi(s)} \tag{8}$$

$$\frac{qV'(s)}{V(s)} = H_1(s) = \frac{K_1 K_2 K_3 \omega'^4 s^2}{\phi(s)} \tag{9}$$

After the putting the value of $V(s)$ in these two equations the equations of $V'(s)$ and $qV'(s)$ are

$$V'(s) = \frac{K_1 K_2 K_3 \omega'^3 s^3}{\phi(s)}\left(\frac{V_{dcoff}}{s} + V_m \frac{\omega}{s^2 + \omega^2}\right) \tag{10}$$

$$qV'(s) = \frac{K_1 K_2 K_3 \omega'^4 s^2}{\phi(s)}\left(\frac{V_{dcoff}}{s} + V_m \frac{\omega}{s^2 + \omega^2}\right) \tag{11}$$

For obtaining the steady sate value of above two equations apply final value theorem

$$v'_\infty(t) = \lim_{t\to\infty} v'(t) = \lim_{s\to 0} sV'(s) \tag{12}$$

$$qv'_\infty(t) = \lim_{t\to\infty} qv'(t) = \lim_{s\to 0} sqV'(s) \tag{13}$$

Ater applying the final value theorem in to the above equations at steady state DC offset which is present in grid voltage will be zero. So, it is concluded that the proposed controller is able to element the DC offset from the grid voltage.

4.2 Generation of PSCs Stage:

In the context of a weak grid, several challenges emerge, including issues related to DC offset, grid harmonics, and grid unbalance. To address these challenges, a novel controller has been proposed. The controller's approach begins by applying Clarke's transformation to convert the three-phase grid voltage (V_{gabc}) into its $\alpha\beta$ component ($V_{\alpha\beta}$). After that SiOGI-FLL controller is used to derive (V'_{α}, V'_{β}) and ($qV'_{\alpha}, qV'_{\beta}$) of α and β. Using these derived parameters, the positive sequence voltages of $\alpha\beta$ is computed ($V^{+}_{\alpha\beta}$).

First, convert the three-phase grid voltage into an $\alpha\beta$ component of the voltage with the help of the following equations.

$$\begin{aligned} V_{\alpha} &= 0.8165\left(V_{ga} - 0.5V_{gb} - 0.5V_{gc}\right) \\ V_{\beta} &= 0.8165\left(0.866V_{gb} - 0.866V_{gc}\right) \end{aligned} \tag{14}$$

now, from the proposed controller find the value of $V'_{\alpha}, qV'_{\alpha}, V'_{\beta}$ and qV'_{β} which are in phase and quadrature component of V_{α} and V_{β}. for calculating the PSCs value of V^{+}_{α} and V^{+}_{β} use the following equation.

$$\begin{aligned} V^{+}_{\alpha} &= 0.5\left(V'_{\alpha} - qV'_{\beta}\right) \\ V^{+}_{\beta} &= 0.5\left(qV'_{\alpha} + V'_{\beta}\right) \end{aligned} \tag{15}$$

Use the following formula to determine the positive sequence grid voltage.

$$\begin{aligned} V^{+}_{ga} &= 0.8165\left(V^{+}_{\alpha} + V^{+}_{\beta}\right) \\ V^{+}_{gb} &= 0.8165\left(-0.5V^{+}_{\alpha} + 0.866V^{+}_{\beta}\right) \\ V^{+}_{gc} &= 0.8165\left(-0.5V^{+}_{\alpha} - 0.866V^{+}_{\beta}\right) \end{aligned} \tag{16}$$

4.3 UVT Calculation

The in phase and quadrature unit vector is calculated by using amplitude of PSCs.

The magnitude of PSCs of grid voltages (V_{tg}) is calculated as follows:

$$V_{tg} = \sqrt{\frac{2}{3}} * \sqrt{V^{+2}_{ga} + V^{+2}_{gb} + V^{+2}_{gc}} \tag{17}$$

The in-phase UVT (u^{+}_{gpa}, u^{+}_{gpb}, and u^{+}_{gpc}) are generated from the grid voltages' estimated PSCs magnitude by using below equation.

$$u_{gpa}^{+}=\frac{V_{ga}^{+}}{V_{tg}},u_{gpb}^{+}=\frac{V_{gb}^{+}}{V_{tg}},u_{gpc}^{+}=\frac{V_{gc}^{+}}{V_{tg}} \tag{18}$$

The grid voltage quadrature UVT constituents are computed using equation 19, which is written as follows.

$$\begin{aligned} u_{gqa}^{+} &= \frac{u_{gpb}^{+}}{\sqrt{3}}+\frac{u_{gpc}^{+}}{\sqrt{3}} \\ u_{gqb}^{+} &= \frac{\sqrt{3}u_{gpa}^{+}}{2}+\frac{\left(u_{gpb}^{+}-u_{gpc}^{+}\right)}{2\sqrt{3}} \\ u_{gqc}^{+} &= -\frac{\sqrt{3}u_{gpa}^{+}}{2}+\frac{\left(u_{gpb}^{+}-u_{gpc}^{+}\right)}{2\sqrt{3}} \end{aligned} \tag{19}$$

4.4 Extraction of Active Weight Component of Load Current and Calculation of I_{net}

The first step for estimating PSCs is to produce the load current in the frame using the expression below.

$$\begin{aligned} I_{\alpha} &= 0.8165\left(I_{La}-0.5I_{Lb}-0.5I_{Lc}\right) \\ I_{\beta} &= 0.8165\left(0.866I_{Lb}-0.866I_{Lc}\right) \end{aligned} \tag{20}$$

$$\begin{aligned} I_{\alpha}^{+} &= 0.5\left(I'_{\alpha}-qI'_{\beta}\right) \\ I_{\beta}^{+} &= 0.5\left(qI'_{\alpha}+I'_{\beta}\right) \end{aligned} \tag{21}$$

$$\begin{aligned} I_{La}^{+} &= 0.8165(I_{\alpha}^{+}+I_{\beta}^{+}) \\ I_{Lb}^{+} &= 0.8165\left(-0.5I_{\alpha}^{+}+0.866I_{\beta}^{+}\right) \\ I_{Lc}^{+} &= 0.8165\left(-0.5I_{\alpha}^{+}-0.866I_{\beta}^{+}\right) \end{aligned} \tag{22}$$

To extract the FC of the load current. Positive sequence current (I_{La}^{+} , I_{Lb}^{+} and I_{Lc}^{+}) are sampled and hold at zero crossing detector unit with the help of UVT quadrature component (u_{gqa}^{+} , u_{gqb}^{+} and u_{gqc}^{+}). And active power component of load current will be (I_a , I_b , and I_c), then calculate the average current (I_{eq}), as indicated in below equation.

$$I_{eq}=\frac{I_a+I_b+I_c}{3} \tag{23}$$

4.4.1 Assessment of the Renewable Feed-Forward Component

To maintain a quick dynamic response in a distribution network, which is crucial given the continuously varying atmospheric conditions and loads, a feed-forward term is a necessity in the control strategy. The renewable feed-forward term is calculated based on the power generated by the renewable energy sources and the voltage amplitude at the Point of Common Coupling (PCC).

equation of renewable energy feed-forward term can represent with the help below equation

$$I_{renff} = \frac{2}{3}\frac{P_{ren}}{V_{tg}} \tag{24}$$

Where I_{renff} represent feed forward term of RESs, where P_{ren} represent RESs power and V_{tg} is magnitude of PSCs of grid voltages.

Simultaneously, the renewable feedforward term, as presented in the result section, aids in controlling the power flow of the system. When solar irradiance is 0 W/m^2, solar PV does not generate any power. In this scenario, power flows from the grid to the load. In other words, the grid meets the load's power demand. When the solar irradiance reaches 1000 W/m^2, solar PV reaches its peak power output. The load initially receives the power from solar PV, while the grid receives the remaining power. Renewable feedforward reduces grid current oscillations in both of these conditions.

4.4.2 Loss Component Evaluation

To avoid faltering during periods of low grid strength and to minimize losses in the converter, the DC link voltage must stabilize rapidly. In order to regulate the output current of the VSC, the DC link voltage must exceed the voltage amplitude at the PCC. A PI controller maintains a stable DC connection voltage during system faults. A PI controller receives the discrepancy between the reference DC link voltage, acquired from the MPPT algorithm, and the observed DC link voltage. The PI controller then calculates the loss component of the converter current.

$$I_{loss} = \left(K_p + \frac{K_i}{s}\right)\left(V_{dc}^* - V_{dc}\right) \tag{25}$$

Where I_{loss} is the output of the PI controller (K_p) proportional gain and (K_i) integral gain represents the gain of the PI controller.

4.4.3 Net Current Calculation

To generate the reference current, total or net current is required, which is the sum of the average value of fundamental load current (I_{eq}), loss component current (I_{loss}) and renewable feedforward current (I_{renff}), which is represented by I_{net}. I_{loss} has been added to this current equation. Moreover, I_{renff} has been subtracted, I_{loss} represents the switching losses of the converter, which also requires to generate an anti-harmonic current. Hence, I_{loss} has been added, and I_{renff} represents the current generated from renewable energy. The power generated from the source is helpful for the power flow with the grid and the load; hence, the I_{renff} term has been subtracted. When the power is not generated from the RESs, then in that condition, the power is supplied to the load from the grid, ensuring continuous power supply. When the RESs generates electricity, power is supplied to the load from RESs, maximizing the use of renewable energy, and the remaining power is supplied to the grid, contributing to the overall power supply.

net current (I_{net}) will be

$$I_{net} = I_{eq} - I_{renff} + I_{loss} \tag{26}$$

4.5 Calculation of Reference Signal

The calculated reference currents (I_{Ca}^*, I_{Cb}^*, and I_{Cc}^*) and actual grid currents (I_{ga}, I_{gb}, and I_{gc}) are fed into the hysteresis current controller, which generates three phase anti-harmonic currents for harmonic mitigation and power enrichment in grid integration renewable energy systems.

$$\begin{aligned} I_{Ca}^* &= I_{net} * u_{gpa}^+ \\ I_{Cb}^* &= I_{net} * u_{gpb}^+ \\ I_{Cc}^* &= I_{net} * u_{gpc}^+ \end{aligned} \tag{27}$$

5 Stability Analysis

The two-way represents the stability of the SiOGI. The first one is represented by plotting its pole-zero plot, which is described in Figure 6. It can be concluded that all the poles of the SiOGI lie on the left-hand side of the imaginary axis, which is why the system is stable. In this plot, out of six poles, four poles lie in a complex conjugate position. Two are in the exact same location on the negative side of the real axis. The second analysis of SiOGI is represented by the root locus of equation 4, which is described in Figure 7. In this plot, there are six root loci. Out of six, two root loci started from an open loop pole and terminated at open loop zero, and the remaining root locus started from an open loop pole and terminated at infinite.

6 Result and Discussion

The entire result and discussion section is divided into two parts. The first part assumes a solar irradiance of 0 W/m^2, while the second part sets it at 1000 W/m^2.

6.1 Simulation Result Under "0 W/m^2" Irradiance Condition

In this scenario, the simulation results demonstrate the elimination of all power quality issues caused by abnormal grid conditions, as well as NLL and UBL conditions, when solar irradiance is 0 W/m^2. In this situation, power flows from the grid to the load.

The MATLAB/Simulink software platform is used to implement the entire system. Table 2 shows the parameters used for the proposed method. The proposed SiOGI-FLL technique is used to examine a grid-connected RESs for PQ improvement at the consumer terminals under steady state with DC offset grid voltage conditions, unbalanced grid voltage, and grid harmonics under linear load (LL), NLL, and UBL. In addition, FFT analysis has been performed in all of these conditions, demonstrating that the controller's performance is quite good in all of these conditions. The suggested SiOGI-FLL is compared with standard approaches, as shown in Tables 3 and 4.

Various types of simulated results generated from the proposed controller under normal grid voltage conditions with LL and NLL conditions are shown in Figures 8 and 9(a). From 0 to 0.2 sec, only NLL is connected after the 0.2-sec LL is also associated. The total harmonic distortion (THD) due to NLL connected before connection to the controller reduced from 28.33% to 2.05% after contact with the controller, which is shown in Figure 9(b) and Figure 9(c), and under both LL and NLL conditions, THD reduced from 18.24% to 0.84%, which is shown in Figure 9(d) and Figure 9(e), and these two cases come under the limit of IEEE-519. In Figure

8, the following parameters are shown, which are as follows: grid voltage (V_{gabc}), three-phase positive sequence grid voltage (V_{gabc}^{+}), positive sequence UVT voltage magnitude (V_{tg}), in-phase and quadrature UVT ($u_{gpabc}^{+}, u_{gqabc}^{+}$), load current($I_{Labc}$), grid current ($I_{gabc}$), net current ($I_{net}$), VSC current ($I_{vsc}$), frequency ($f$), phase angle in radian (θ). From Figure 8, it is concluded that the proposed controller is capable of reducing the harmonics produced by the NLL. The grid current will always be sinusoidal, and throughout the operation, the frequency of the grid will be 50 Hz. From 0.2 seconds on, the LL is also connected to the NLL. That is why the magnitude of load current is also increased, and the magnitude of I_{net} will be greater after 0.2 seconds. Figure 9(a) shows the remaining parameters of the controller under normal grid voltage conditions, which are not present in Figure 8. The simulated results in this figure are the compensated reference current (I_{Cabc}^{*}), the $\alpha\beta$ component of grid voltage ($V_{\alpha\beta}$) and load current ($I_{\alpha\beta}$), and the positive sequence $\alpha\beta$ component of grid voltage ($V_{\alpha\beta}^{+}$) and load current ($I_{\alpha\beta}^{+}$). There is no abnormality in normal grid voltage conditions, so the $\alpha\beta$ component of the grid voltage is standard. Still, due to NLL, harmonics are present in the $\alpha\beta$ component of load current ($I_{\alpha\beta}$), but when the controller is connected, all these harmonics are removed.

6.1.1 Grid Voltage with Presence of DC Offset

DC offset is a significant reason for increasing PQ issues, so removing DC offset from the grid becomes essential to solve all kinds of power quality problems. The main reasons for DC offset in the grid are the presence of unbalanced loads, asymmetrical faults, non-linear loads, transformer magnetization, and ground issues. Due to the presence of DC offset in the power grid, various adverse effects are produced. This is as follows: increase in losses, decrease in efficiency, increase in stress in electrical equipment, impact on multiple types of sensitive electronics equipment, so it is necessary to remove DC offset from the grid. Figure 10(a) shows the different types of results produced by the presence of DC offset in the grid, which are respectively three-phase grid voltage with DC component (V_{gabc}), three-phase positive sequence voltage (V_{gabc}^{+}) produced after applying the proposed controller, load current(I_{Labc}), grid current (I_{gabc}), compensation current (I_{Cabc}^{*}), VSC current (I_{vsc}), which is anti-harmonics current, $\alpha\beta$ component of grid voltage($V_{\alpha\beta}$), positive sequence $\alpha\beta$ component of grid voltage ($V_{\alpha\beta}^{+}$), $\alpha\beta$ component of load current ($I_{\alpha\beta}$), positive sequence $\alpha\beta$ component of load current ($I_{\alpha\beta}^{+}$). In the Figure 10(a), an NLL is connected from 0 to 0.2 sec and after 0.2 seconds LL is also attached. THD in load current due to DC offset in the grid is 28.44% in NLL conditions. THD due to LL and NLL is 18.31% which is represented in Figure 10(b) and Figure 10(c), which is reduced to 1.77% and 0.94% by connecting the controller, which is described in Figure 10(d) and Figure 10(e). Figure 10(a) shows the effect of DC offset in the $\alpha\beta$ component of the grid voltage, in which the quadrature sequence component in the $\alpha\beta$ element in the grid voltage is slightly higher due to the presence of the DC component in the grid voltage. And this DC component is filtered after connecting the proposed controller. Similarly, in the figure, an $\alpha\beta$ component of load current ($I_{\alpha\beta}$) is also shown. Before joining the controller, the harmonics generated due to NLL are present in this $\alpha\beta$ component, and after connecting the proposed controller, these harmonics components are filtered.

6.1.2 Grid Voltage with Harmonics

Various types of power quality problems arise due to the harmonic's component in grid voltage. There are multiple reasons for the harmonics component in grid voltage, such as NLL presence, arc furnace, lighting system, phase unbalance, capacitor switching, and system resonance. Therefore, eliminating grid harmonics becomes imperative. Figure 11(a) shows the simulation result the condition of grid harmonics. The simulation result lists the different types of results, which are three-phase grid voltage with harmonics (V_{gabc}), (V_{gabc}^{+}), (I_{Labc}), (I_{gabc}), (I_{Cabc}^{*}), three-phase VSC current (I_{vsc}), the $\alpha\beta$ component of grid voltage ($V_{\alpha\beta}$) and load current ($I_{\alpha\beta}$) and positive sequence $\alpha\beta$ component of grid voltage ($V_{\alpha\beta}^{+}$) and load current ($I_{\alpha\beta}^{+}$). In Figure 11(a), from 0 to 0.2 sec, only the NLL is connected, and after 0.2 sec, the LL is also attached. THD due to NLL and grid harmonics 38.19%, which is reduced to 2.42% after connecting the controller, as shown in Figure 11(b) and Figure 11(c) and THD is 32.80% due to connecting both LL and NLL have reduced to 1.10%, which is shown in Figure 11(d) and Figure 11(e). The effect of grid harmonics can also be seen in the $\alpha\beta$ component of the voltage and after connecting the proposed controller the effect of harmonics is eliminated. The impact of NLL and grid harmonics is also shown in the figure 11 (a) in the form of $\alpha\beta$ current of load current ($I_{\alpha\beta}$), and after connecting the controller, is effect is also eliminated.

6.1.3 Grid Unbalance Condition

Grid unbalance, also known as electrical unbalance, occurs when an unequal distribution of load or power among the phases in an electrical power are different. This phenomenon can have various reasons, including some common causes for grid unbalance. Asymmetrical loads, single-phase loads, motor starting, unbalanced distribution transformers, faults and short circuits, phase shift in transformers, neutral conductor issues, voltage imbalance, unbalanced generation, and grid unbalance can have adverse effects on power system equipment, including motors, transformers, and other electrical components. It can cause overheating, increased losses, reduced efficiency, and even equipment failure. Therefore, it is essential to solve the problem of grid unbalance, which can be solved with the help of the proposed controller. Figure 12(a) shows the simulated results under grid unbalance conditions, which are respectively, three-phase unbalanced grid voltage (V_{gabc}), (V_{gabc}^{+}), (I_{Labc}), (I_{gabc}), (I_{Cabc}^{*}), VSC current (I_{vsc}), ($V_{\alpha\beta}$),($I_{\alpha\beta}$), ($V_{\alpha\beta}^{+}$) and ($I_{\alpha\beta}^{+}$). The grid voltage has been generated with the help of MATLAB/Simulink software, in which the voltage of the three phases of the three-phase grid is different. After implementing the proposed controller, a three-phase positive sequence grid voltage is generated (V_{gabc}^{+}) in which the voltage of all three grid phases is the same. Before applying the proposed controller, the effect of grid unbalance can be seen in the $\alpha\beta$ component of grid voltage ($V_{\alpha\beta}$). In this result, the value of the quadrature component of grid voltage is more than the direct axis component, and after applying the proposed controller, the quadrature and direct axis components have equal values. Due to an NLL, harmonics are present in ($I_{\alpha\beta}$), which is eliminated after applying the proposed controller. Finally, after using the proposed controller, the grid current has become completely sinusoidal; it can be understood with the help of FFT analysis, which is shown in Figure 12(b), 12(c), 12(d), and 12(e). Grid current before applying the controller THD are 25.24% and 16.22%, due to NLL and both LL and NLL, which have reduced to 2.02% and 0.96%, respectively, after applying the controller.

6.1.4 Unbalance Load Condition

Figure 13 presents the simulation results under unbalanced load and grid voltage conditions, showcasing variables such as unstable grid voltage, positive sequence components, load current, and VSC current. Initially, the grid voltage and load current are unbalanced, as evidenced by the differing magnitudes of the direct and quadrature axis components. After applying the proposed controller, both grid voltage and load current achieve balance, with equalized magnitude components. Notably, the VSC current waveform differs in the absence of NLL. The results confirm the controller's effectiveness in mitigating unbalanced conditions and restoring system stability.

6.2 Simulation Result Under 1000 *W/m²* Irradiance Condition

This condition illustrates a variety of power quality issues that can arise in the grid, as well as abnormal load conditions when solar PV is present.

6.2.1 DC-Offset Condition with 1000 *W/m²* Irradiance

Figure 14(a) shows the simulation results generated under the grid with a DC offset and a solar PV condition. This simulation result shows five waveforms: three-phase grid voltage with DC offset, three-phase load current, three-phase grid current, three-phase VSC current, and DC link voltage, respectively. Under this condition, the supply of power from solar PV to the load and grid is completely sinusoidal, resulting in a THDs of 0.24%, for normal grid and 1.35%, for DC offset condition, in line with the IEEE standard as illustrated in Figure 14(b) and Figure 14(c) respectively.

6.2.2 Grid Voltage with Harmonics with 1000 *W/m²* Irradiance

Figure 15(a) shows the simulation result for grid voltage under harmonics with solar PV. The MATLAB/Simulink software generates harmonics by utilizing a three-phase programmable voltage source block to add the 3^{rd} and 5^{th} harmonics to the grid voltage. This figure displays five waveforms, demonstrating a perfectly sinusoidal grid current in the third wave of Figure 15(a) and a THD of 1.39% in Figure 15(b).

6.2.3 Grid Unbalance with 1000 *W/m²* Irradiance

Figure 16(a) shows the grid imbalance under the solar PV condition. To illustrate the unbalanced grid, MATLAB/Simulink software uses a three-phase source block. This figure also showcases five distinct waveforms. Under this condition, the third wave form of Figure 8(f) illustrates the grid current's perfect sinusoidal, with a THD content of 0.25%, in line with the IEEE standard, as illustrated in Figure 16(b).

6.2.4 Sag and Swell Condition

In a grid-connected solar PV system, "sag" and "swell" refer to short-duration variations in the voltage level. These events can affect the performance and stability of the system. Voltage sags (also known as dips) are characterised by a short-term reduction in the RMS voltage level, typically lasting from a few milliseconds to a few seconds. Sags are frequently caused by high load starts, power system faults, network configure ration changes, and lightning strikes. Swells are commonly caused by load shedding, fault clearing, switching operations, and lightning strikes. Figure 17(a) shows the simulation results generated under sag and swell conditions. MATLAB/Simulink software uses a three-phase programmable voltage source to generate the sag and swell conditions. The figure shows five waveforms, demonstrating a perfectly sinusoidal grid current under sag and swell conditions. Figure 17(b) and 17(c) display the FFT analysis, revealing a value of less than 5%. In Figure 17 (*a's* third wave form), the grid current has increased in the sag condition and decreased in the swell condition. The main reason for this is that when the voltage decreases in the sag condition, the load current also decreases. As a result, solar PV supplies less power to the load, with the grid receiving the majority of it. In the swell condition, an increase in voltage necessitates an increase in load current, resulting in a decrease in power supply from the solar PV to the grid.

6.2.5 Variable Solar Irradiance Condition

Variable solar irradiance refers to fluctuations in sunlight reaching a solar PV system, primarily caused by environmental factors such as clouds, weather patterns, and atmospheric conditions. Different regions experience varying degrees of solar irradiance variability, impacting the performance and stability of grid-connected solar PV systems. Here’s a list of bad impacts in grid-connected solar PV systems: power quality issues (voltage fluctuations, frequency variations), reduced efficiency (inverter efficiency, mismatch losses), increased wear and tear

(equipment stress, battery degradation), grid stability challenges, and economic impacts. Figure 18 shows the different simulation results generated under variable irradiance conditions. We use the signal builder block of MATLAB/Simulink software to generate variable irradiance. We set the solar irradiance in this simulation to 1000 W/m^2 between 0 and 0.05 seconds, 0.35 to 0.45 seconds, and 600 W/m^2 between 0.05 and 0.15 seconds, 0.25 to 0.35 seconds. We set the solar irradiance to 0 W/m^2 for a duration of 1.5 to 0.25 seconds. This figure shows 8 different waveforms, which are respectively solar irradiance, PV current, PV voltage, PV power, voltage source converter output power, load power, grid power, and grid current. As solar irradiance changes, PV current and power also change. When the solar irradiance falls between 1000 W/m^2 and 600 W/m^2, the load power remains constant. In this scenario, the load receives solar-generated power, while the grid receives the remaining power. The negative seventh waveform of Figure 18 clearly demonstrates the supply of solar PV-generated power to the grid. However, when the solar irradiance is zero, solar PV ceases to generate no power. Consequently, the grid supplies power to the load, as indicated by the positive seventh waveform in this figure. The grid current is always sinusoidal, irrespective of variations in solar irradiance.

6.2.6 Power Factor

In the context of grid-connected solar PV systems, "power factor" refers to the ratio of real power (measured in watts) to apparent power (measured in volt-amperes). A poor power factor indicates inefficiencies in the system, often caused by reactive power, which does not contribute to useful work but creates additional load on the grid. Connecting solar power to the grid only allows the solar panel to meet the load's active power demand, not the reactive power demand, resulting in a decrease in the system's power factor. The proposed controller is capable of solving this problem. This section determines the power factor of the grid. This section determines the grid's power factor by applying the controller to various abnormal grid and load conditions, as illustrated in figure 19. This figure shows the power factor under five different conditions: a normal grid condition with a non-linear load, a grid voltage with harmonics, a grid voltage with a DC offset, an unbalanced grid voltage, a sag, and a swell condition. By using the proposed controller, the grid's power factor has improved to almost unity.

7 Comparative Analyses

The comparison analysis of the proposed controller is done based on the bode plot. Various controllers like SOGI, ISOGI, MSTOGI, CSOGI, SOSOGI, CNISOGI, FOGI, and the proposed controller, which is the SiOGI. A bode plot is plotted, which is shown in Figure 20(a). It is observed from Figure 20(a) that for low frequencies, the magnitude of the Bode plot of the direct axis Sixth-OGI(s) and quadrature Sixth-OGI(s) lies very below, which indicates more attenuation of the DC component and low-frequency components as compared to other control techniques. The performance of a SiOGI is tested on an unbalanced grid with polluted grid voltage, which suffers from DC offset, undervoltage, overvoltage, and harmonic distortions. The step response of the ISOGI, MSTOGI, CSOGI, SOSOGI, CNISOGI, and Sixth-OGI is shown in Figure. 20(b). From the step response, it is concluded that the system’s settling time is low compared to the other controller. Table 3 summarizes the suggested technique’s comparison with SOGI, ISOGI, MSTOGI, CSOGI, SOSOGI, CNISOGI, and FOGI approaches. The SiOGI-FLL method outperforms all other techniques under grid harmonics, DC offset, and unbalanced grid conditions with LL, NLL, and UBL conditions. The THD due to the proposed controller are 1.60%, 1.43%, and 1.77% under grid harmonics, dc offset, and both grid harmonics and dc offset conditions, respectively, which are good compared to another controller. Furthermore, the suggested controller was compared to the present controller in terms of oscillation, amplitude tracking, frequency tracking, phase tracking, fundamental tracking, grid synchronization, accuracy, DC offset elimination, overshoot, static error, and settling time. The suggested controller outperforms all other controllers in all these criteria. Simultaneously, this research paper compares the proposed controller with the conventional controllers used in real-world scenarios. Table 4 displays the use of IRPT, SRF, fryze, and ADALINE controllers as conventional controllers. This table compares all power quality issues that arise from connecting the grid to renewable energy, including voltage fluctuation, harmonics mitigation, frequency deviation, power factor, balancing, accuracy, DC offset elimination, flicker, harmonics under sag and swell conditions, both current and voltage harmonics mitigation capabilities, and fundamental current extraction.

8 Conclusion

This research paper has presented a comprehensive investigation into a new controller to enhance power quality in electrical systems operating under various weak grid conditions. The identified power quality issues, including DC offset, unbalanced grid voltages, grid harmonics, and the presence of LL, NLL and UBL, pose significant challenges to power systems' reliable and efficient operation. Through an in-depth analysis of the existing power quality problems and their associated impacts on system performance, the proposed controller offers a robust and innovative solution to mitigate these issues effectively. The critical contribution of this research lies in developing an adaptive and intelligent control algorithm capable of dynamically adjusting system parameters and responding to grid and load conditions in real time. The simulation results demonstrate the efficacy of the new controller in achieving significant improvements in power quality, as evidenced by reduced harmonic distortion, enhanced voltage balance, and minimized DC offset. The controller's adaptability and ability to handle multiple challenging scenarios contribute to its practical applicability in a wide range of weak grid environments. While this study successfully addresses the outlined PQ issues under various weak grid conditions, it also opens up new opportunities for further research. Areas of future exploration include integrating RESs, considering advanced control techniques, and developing innovative grid technologies, all of which will contribute to a more resilient and sustainable power infrastructure. Ultimately, with continued research and development in this field, it can aspire to achieve a cleaner, more efficient, and more reliable power supply for generations to come.

Acknowledgement

This work is carried out in the power electronics laboratory of the School of Electrical and Electronics Engineering VIT Bhopal University, Sehore, INDIA.

References

[1] Suvorov, Aleksey, Alisher Askarov, et al. "Comparative small-signal stability analysis of voltage-controlled and enhanced current-controlled virtual synchronous generators under weak and stiff grid conditions." International Journal of Electrical Power & Energy Systems, 147, p. 108891 (2023). https://doi.org/10.1016/j.ijepes.2022.108891.

[2] Jha, K., & Shaik, A. G. A" Comprehensive review of power quality mitigation in the scenario of solar pv integration into utility grid". e-Prime-Advances in Electrical Engineering, Electronics and Energy, 3, p. 100103 (2023). https://doi.org/10.1016/j.prime.2022.100103.

[3] Kumar, R. S., Prabakaran, S., & Selvan, S. S." Adaptive control of grid integrated photovoltaic using recurrent neural network". International Journal of Intelligent Systems and Applications in Engineering, 11(6s), pp. 295-300 (2023). https://ijisae.org/index.php/IJISAE/article/view/2856.

[4] Badoni, M., Singh, A., Singh, A. K., et al." Grid tied solar pv system with power quality enhancement using adaptive generalized maximum versoria criterion". CSEE Journal of Power and Energy Systems, 9(2), pp. 722-732 (2021). DOI: 10.17775/CSEEJPES.2020.04820.

[5] Xue, C., Ding, L., & Li, Y." Improved model predictive control with reduced dc-Link capacitor rms current for back-to-back converter-fed PMSM drives". IEEE Transactions on Industrial Electronics, 71(1), pp.194-203, (2023). DOI: 10.1109/TIE.2023.3243288.

[6] Tuyen ND, Fujita G. Pv-active power filter combination supplies power to nonlinear load and compensates utility current. IEEE Power and Energy Technology Systems Journal, 2(1), pp.32-42 (2015). DOI: 10.1109/JPETS.2015.2404355.

[7] Lakshmanan, S. A., Rajpurohit, B. S., & Jain, A. "Optimum setting algorithm-based pi controller tuning for SRF-PLL used grid synchronization system", Electric Power Components and Systems, 51(6), pp.538-554 (2023). https://doi.org/10.1080/15325008.2023.2178544

[8] Latha, H. S., Sujatha, K. N., & Radhika, G." A novel approach of hybrid active power filter using fryze current controller". In 2021 6th International Conference on Communication and Electronics Systems (ICCES), pp. 348-352 (2021) IEEE. DOI: 10.1109/ICCES51350.2021.9489150.

[9] Chawda, G. S., & Shaik, A. G. "Enhancement of wind energy penetration levels in rural grid using adaline-lms controlled distribution static compensator", IEEE Transactions on Sustainable Energy, 13(1), pp.135-145 (2021). DOI: 10.1109/TSTE.2021.3105423.

[10] Srikanth, I., & Kumar, P. (2023)." Neural network based dstatcom control for Power Quality Enhancement". In Robotics, Control and Computer Vision: Select Proceedings of ICRCCV. Singapore: Springer Nature Singapore, pp.313-322 (2022), https://doi.org/10.1007/978-981-99-0236-1_25.

[11] Çelik, D., Ahmed, H., & Meral, M. E. "Kalman filter-based super-twisting sliding mode control of shunt active power filter for electric vehicle charging station applications". IEEE Transactions on Power Delivery, 38(2), pp.1097-1107 (2022), DOI: 10.1109/TPWRD.2022.3206267.

[12] Pattanaik, D., Swain, S. C., Samanta, I. S., et al." Synchronized wavelet transform based power quality disturbance detection and monitoring of solar integrated micro-grid". In International Conference on Power Electronics and Energy (ICPEE), pp. 1-6 (2023) IEEE. DOI: 10.1109/ICPEE54198.2023.10060530.

[13] Priyadarshini, M. S., Krishna, D., Kumar, K. V., et al." Significance of harmonic filters by computation of short-time fourier transform-based time–frequency representation of supply voltage. energies", 16(5), pp 2194 (2023), https://doi.org/10.3390/en16052194.

[14] Kumar, A., & Kumar, P." Power quality improvement for grid-connected PV system based on distribution static compensator with fuzzy logic controller and uvt/adaline-based least

mean square controller", Journal of Modern Power Systems and Clean Energy, 9(6), pp 1289-1299 (2021), 10.35833/MPCE.2021.000285.

[15] Alam, S. J., & Arya, S. R." Volterra lms/f-based control algorithm for upqc with multi-objective optimized PI controller gains", IEEE Journal of Emerging and Selected Topics in Power Electronics, 11(4), pp.4368-4376 (2022). DOI: 10.1109/JESTPE.2022.3146210.

[16] Dey, D., & Subudhi, B.A. "Normalized least means absolute third-based adaptive control algorithm design for grid-connected PV system". IEEE Journal of Emerging and Selected Topics in Power Electronics, 11(2), pp 2291-2299 (2022), DOI: 10.1109/JESTPE.2022.3220247.

[17] Somalwar, R. S., Kadwane, S. G., & Ruikar, J. "Advanced active islanding method with recursive least square for microgrid". IEEE Journal of Emerging and Selected Topics in Industrial Electronics., (2024). DOI: 10.1109/JESTIE.2023.3274476.

[18] Jalal, B., Yang, X., Liu, Q., et al. "Fast and robust variable-step-size lms algorithm for adaptive beamforming". IEEE Antennas and Wireless Propagation Letters, 19(7), pp. 1206-1210 (2020). DOI: 10.1109/LAWP.2020.2995244.

[19] Singh, B., Jain, C., & Goel, S." Ilst control algorithm of single-stage dual purpose grid connected solar pv system". IEEE Transactions on Power Electronics, 29(10), pp 5347-5357 (2013), DOI: 10.1109/TPEL.2013.2293656.

[20] Somkun, S., Srita, S., Kaewchum, T., et al." Adaptive notch filters for bus voltage control and capacitance degradation prognostic of single-phase grid-connected inverter". IEEE Transactions on Industrial Electronics, 70(12), pp.12190-12200 (2023), DOI: 10.1109/TIE.2023.3237904.

[21] Althobaiti, A., Ullah, N., Belkhier, Y., et al." Expert knowledge based proportional resonant controller for three phase inverters under abnormal grid conditions". International Journal of Green Energy, 20(7), pp 767-783 (2023), https://doi.org/10.1080/15435075.2022.2107395.

[22] Xu, J., Qian, H., Qian, Q., et al. “Modeling, stability, and design of the single-phase sogi-based phase-locked loop considering the frequency feedback loop effect”. IEEE Transactions on Power Electronics, 38(1), pp.987-1002 (2022). DOI: 10.1109/TPEL.2022.3201252.

[23] Golestan, S., Guerrero, J. M., Vasquez, J. C., et al.” Modelling, tuning, and performance comparison of second-order-generalized integrator-based FLLs”. IEEE Transactions on Power Electronics, 33(12), pp. 10229-10239 (2018), DOI: 10.1109/TPEL.2018.2808246.

[24] Narayanan, V., & Singh, B.” Sogi-fll-wdcrc filter for seamless control of microgrid for optimal coordination of conventional and renewable energy resources”. IEEE Transactions on Industry Applications, 59(4), pp.4821-4834 (2023), DOI: 10.1109/TIA.2023.3261869.

[25] Shah, P., Hussain, I., & Singh, B.” Single-stage secs interfaced with grid using isogi-fll-based control algorithm”. IEEE Transactions on Industry Applications, 55(1), pp 701-711 (2018). DOI: 10.1109/TIA.2018.2869880.

[26] Babu, N., Guerrero, J. M., Siano, P., et al.” An improved adaptive control strategy in grid-tied pv system with active power filter for power quality enhancement”. IEEE Systems Journal, 15(2), pp 2859-2870 (2020), DOI: 10.1109/JSYST.2020.2985164.

[27] Jain, V., & Singh, B. (2018). “A multiple improved notch filter-based control for a single-stage pv system tied to a weak grid”. IEEE Transactions on Sustainable Energy, 10(1), pp. 238-247 (2018). DOI: 10.1109/TSTE.2018.2831704.

[28] Zhang, C., Zhao, X., Wang, X., et al.” A grid synchronization pll method based on mixed second-and third-order generalized integrator for dc offset elimination and frequency adaptability”. IEEE Journal of Emerging and Selected Topics in Power Electronics, 6(3), pp 1517-1526 (2018). DOI: 10.1109/JESTPE.2018.2810499.

[29] Chakraborty, S., Modi, G., & Singh, B.” Mstogi-fll-rogi based frequency adaptive control for a single stage spva-bes-bdc-dg set connected standalone microgrid for remote areas”. IEEE Transactions on Industry Applications, 59(3), pp.3727-3740 (2023), DOI: 10.1109/TIA.2023.3247403.

[30] Naqvi, S. B. Q., & Singh, B.” An enhanced filtering generalized integrator-based control for improved performance of a grid tied pv system at adverse grid voltages”. IEEE

Transactions on Industrial Electronics, 70(12), pp.12376-12386 (2023), DOI: 10.1109/TIE.2023.3239922.

[31] Modi, G., and Singh, B.” Improved cascaded sogi control for islanding synchronization in photovoltaic system”. IEEE Transactions on Industry Applications, 58(6), pp 6909-6919 (2022), DOI: 10.1109/TIA.2022.3201808.

[32] Mondal, B. and Karuppaswamy, B. A. "A new approach to fourth-order quadrature signal generation for a fast and noise-free pll output under non-ideal grid voltage conditions," in *IEEE Access*, 10, pp. 38472-38482 (2022), doi: 10.1109/ACCESS.2022.3165561.

[33] Narayanan, V., & Singh, B.” Cnisogi and vssmclms filters for solving grid and load abnormalities for a microgrid with seamless mode transfer capability”. IEEE Transactions on Industry Applications, 59(4), pp. 4225-4237 (2023), DOI: 10.1109/TIA.2023.3259387.

[34] Ogata, K. “Modern control engineering”, vol. 3, 5th ed., pp. 189–192, Pearson, London, U.K., (2015).

[35] Babu, P. N., Peesapati, R., & Panda, G.”An adaptive differentiation frequency based advanced reference current generator in grid-tied pv applications”. IEEE Journal of Emerging and Selected Topics in Power Electronics, 8(4), pp 3502-3515 (2019), DOI: 10.1109/JESTPE.2019.2933140.

Figure and Table Captions

Figure Captions

Figure 1 Proposed structure of grid-tied renewable energy systems
Figure 2 Complete control block diagram
Figure 3 Sixth order generalized integrator-frequency locked loop (SiOGI-FLL)
Figure 4 Flow Chart
Figure 5 Step response at different value of controller gain
Figure 6 Pole-Zero plot of sixth order generalized integrator transfer function
Figure 7 Root locus plot of sixth order generalized integrator transfer function
Figure 8 Simulation result of controller under normal grid voltage condition

Figure 9 Results under normal grid voltage condition (a) Simulation, (b) FFT for NLL without controller, (c) FFT for NLL with controller, (d) FFT for both LL and NLL without controller, (e) FFT for both LL and NLL with controller

Figure 10 Results under grid voltage with DC offset condition, (a) Simulation, (b) FFT for NLL without controller, (c) FFT for LL and without Controller, (d) FFT for NLL with controller, (e) FFT for LL and NLL with controller

Figure 11 Results under grid voltage with harmonics condition, (a) Simulation, (b) FFT for NLL without controller, (c) FFT for NLL with controller, (d) FFT for both LL and NLL without controller, (e) FFT for both LL and NLL with controller

Figure 12 Results under unbalanced grid voltage condition (a) Simulation, (b) FFT for NLL without controller, (c) FFT for NLL with controller, (d) FFT for both LL and NLL without controller, (e) FFT for both LL and NLL with controller

Figure 13 Simulation result unbalance grid voltage condition with unbalanced load

Figure 14 Results under grid voltage with DC offset condition, (a) Simulation, (b) FFT for healthy grid with controller, (c) FFT for DC offset with controller

Figure 15 Results under grid voltage with harmonics condition, (a) Simulation, (b) FFT with controller

Figure 16 Results under unbalanced grid voltage condition (a) Simulation, (b) FFT with controller,

Figure 17 Results under sag and swell condition (a) Simulation, (b) FFT for sag, (c) FFT for swell

Figure 18 Simulation under variable solar irradiance condition

Figure 19 Power factor under various grid voltage condition

Figure 20 Comparative curve for quadrature axis transfer function, (a) Bode plot, (b) Step response

Table Captions

1. Table 1 Abbreviations and its full form
2. Table 2 Specification of the system
3. Table 3 Comparative analysis
4. Table 4 Comparative analysis with conventional controller

Figures: -

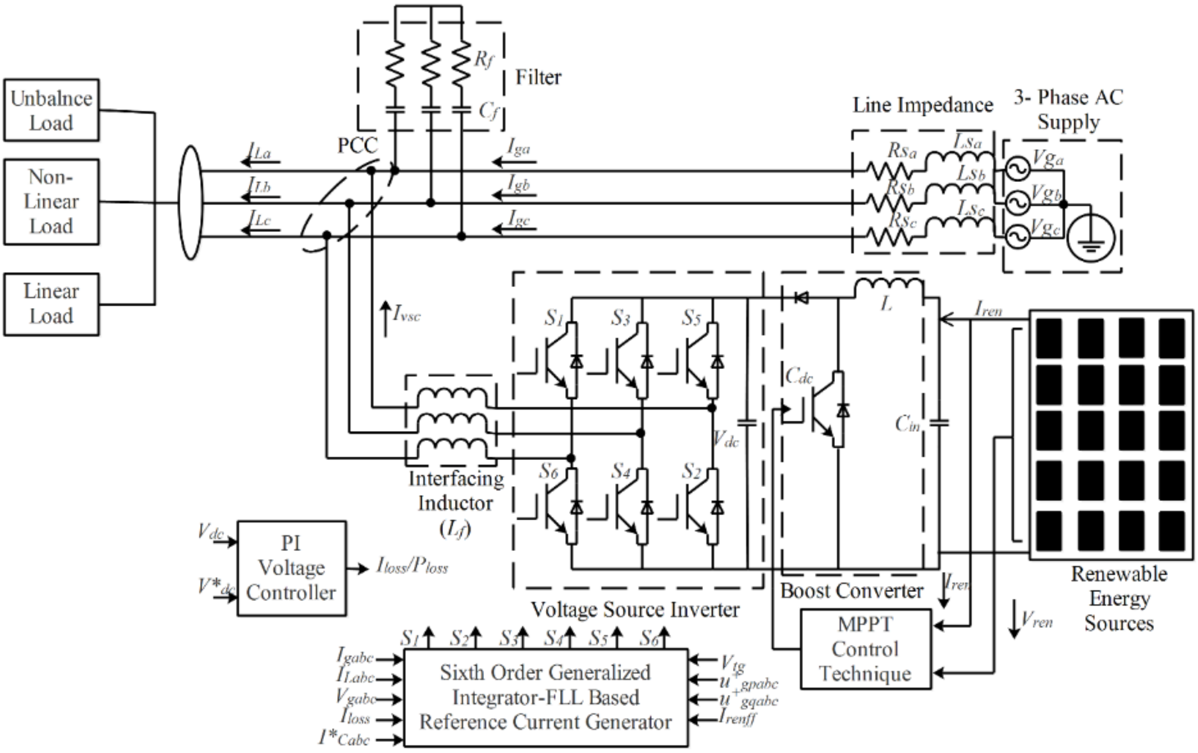

Figure 1 Proposed structure of grid-tied renewable energy systems

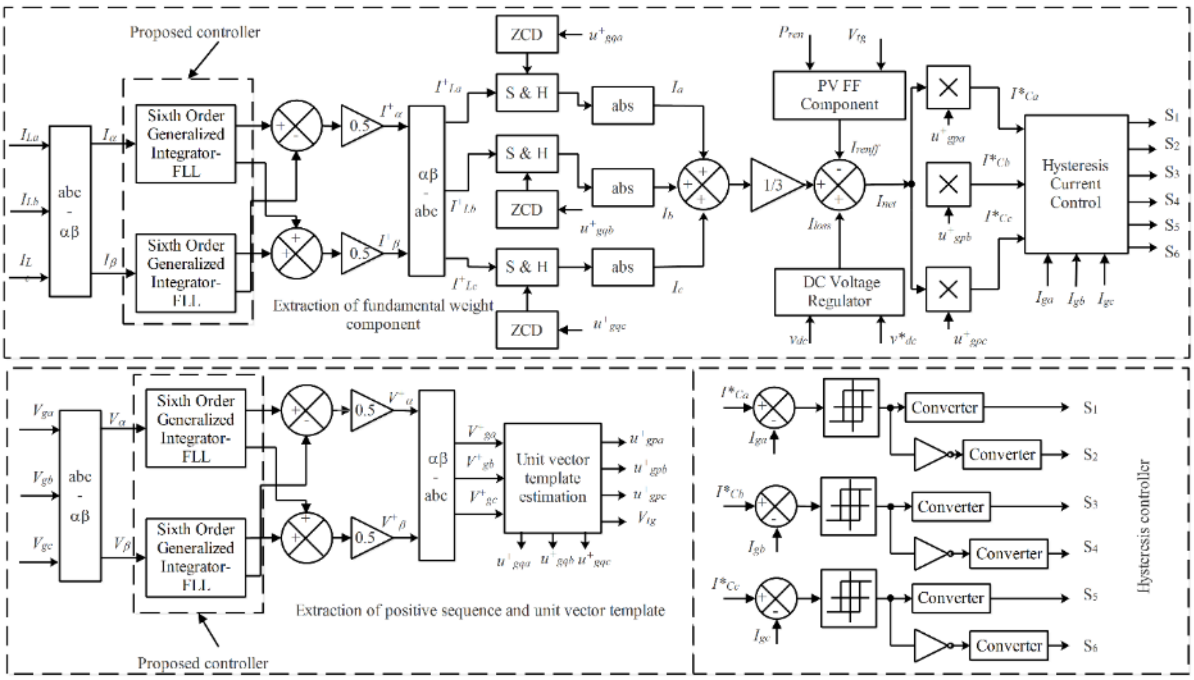

Figure 2 Complete control block diagram.

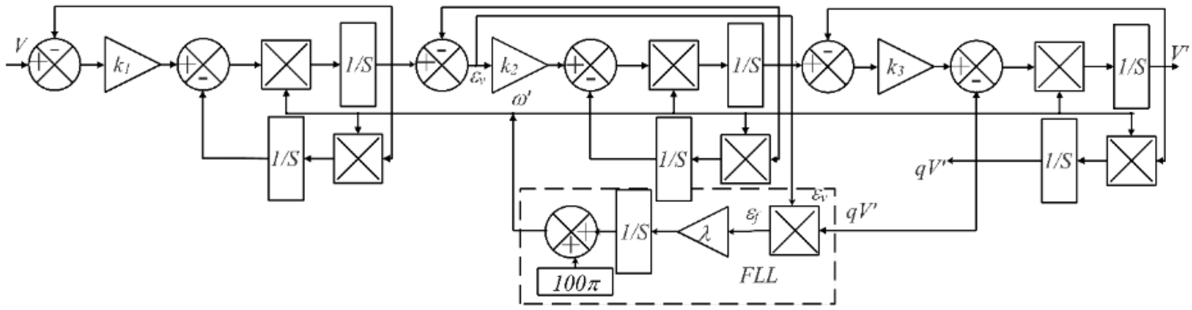

Figure 3 Sixth order generalized integrator-frequency locked loop (SiOGI-FLL)

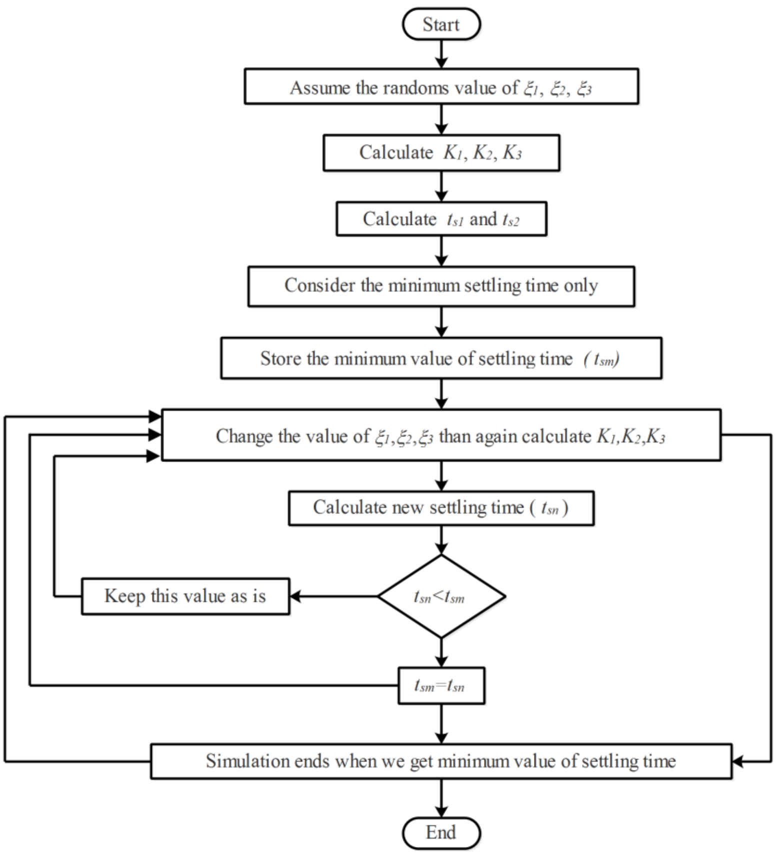

Figure 4 Flow chart

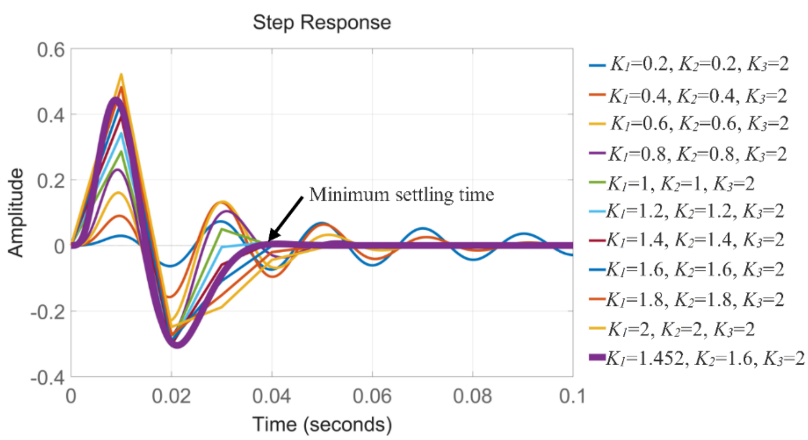

Figure 5 Step response at different value of controller gain

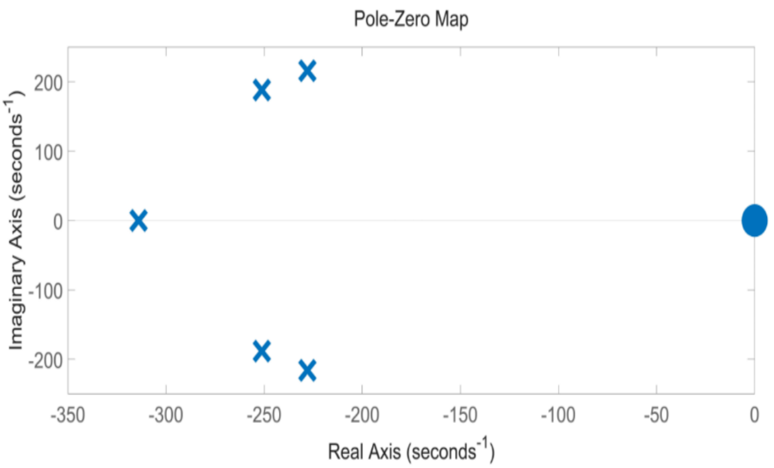

Figure 6 Pole-zero plot of SiOGI transfer function

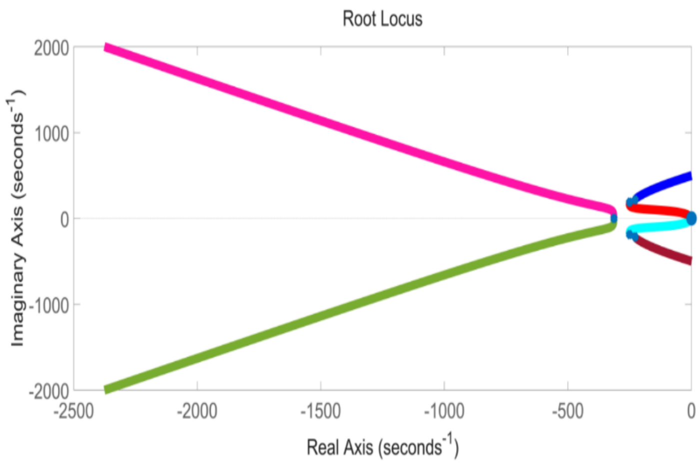

Figure 7 Root locus plot of SiOGI transfer function

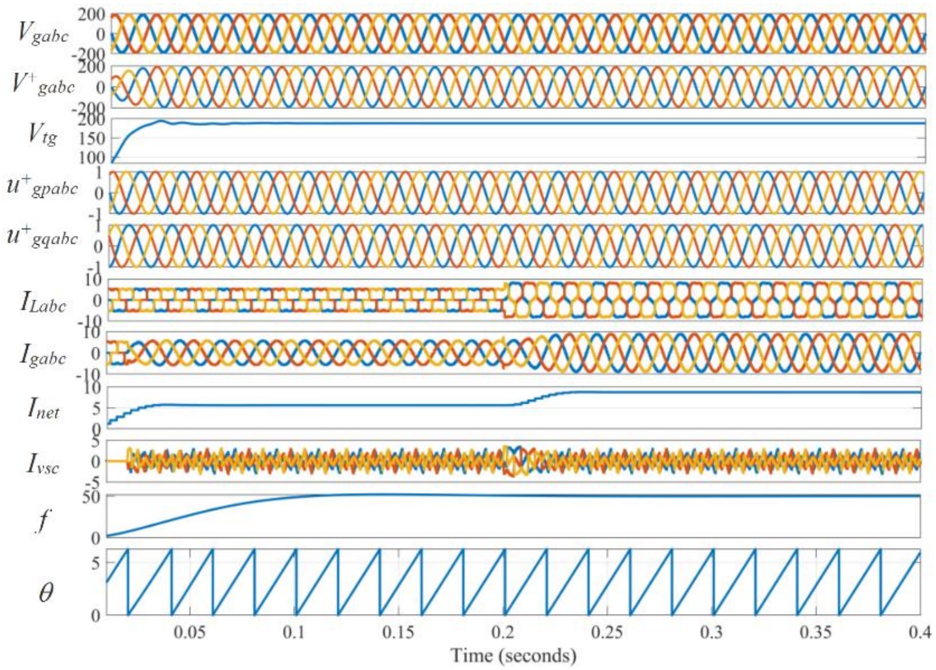

Figure 8 Simulation result of controller under normal grid voltage condition

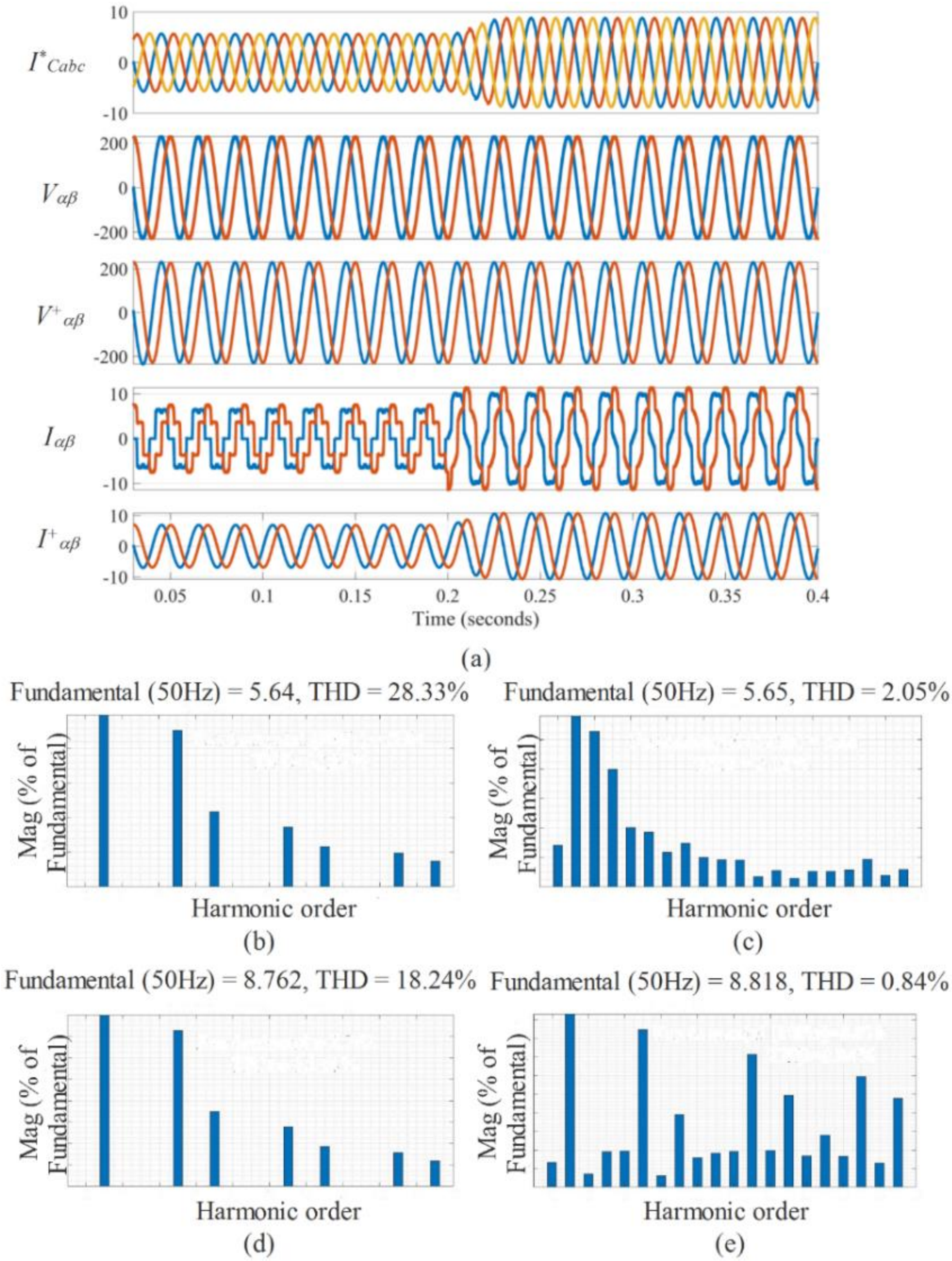

Figure 9 Results under normal grid voltage condition (a) Simulation, (b) FFT for NLL without controller, (c) FFT for NLL with controller, (d) FFT for both LL and NLL without controller, (e) FFT for both LL and NLL with controller

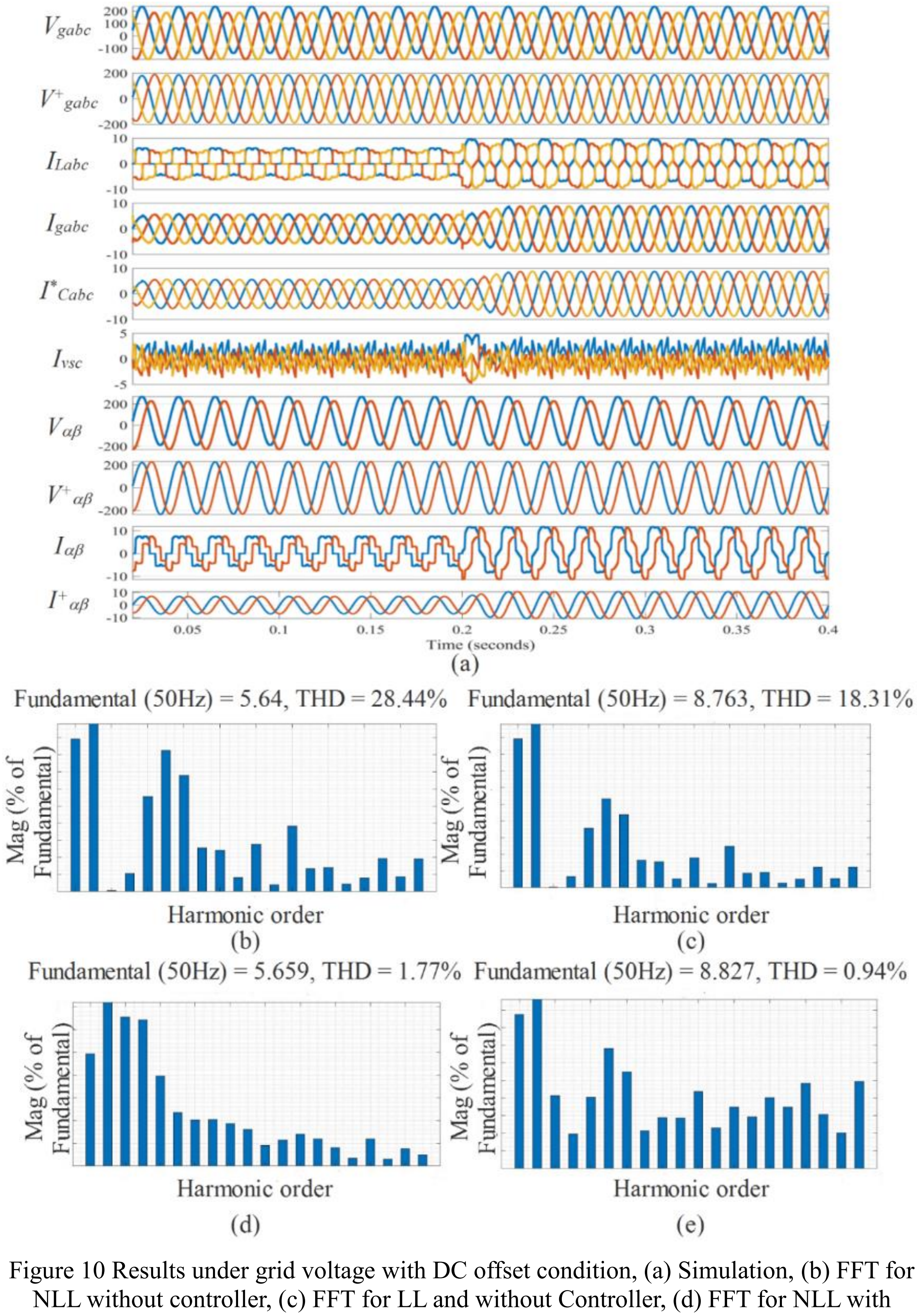

Figure 10 Results under grid voltage with DC offset condition, (a) Simulation, (b) FFT for NLL without controller, (c) FFT for LL and without Controller, (d) FFT for NLL with controller, (e) FFT for LL and NLL with controller

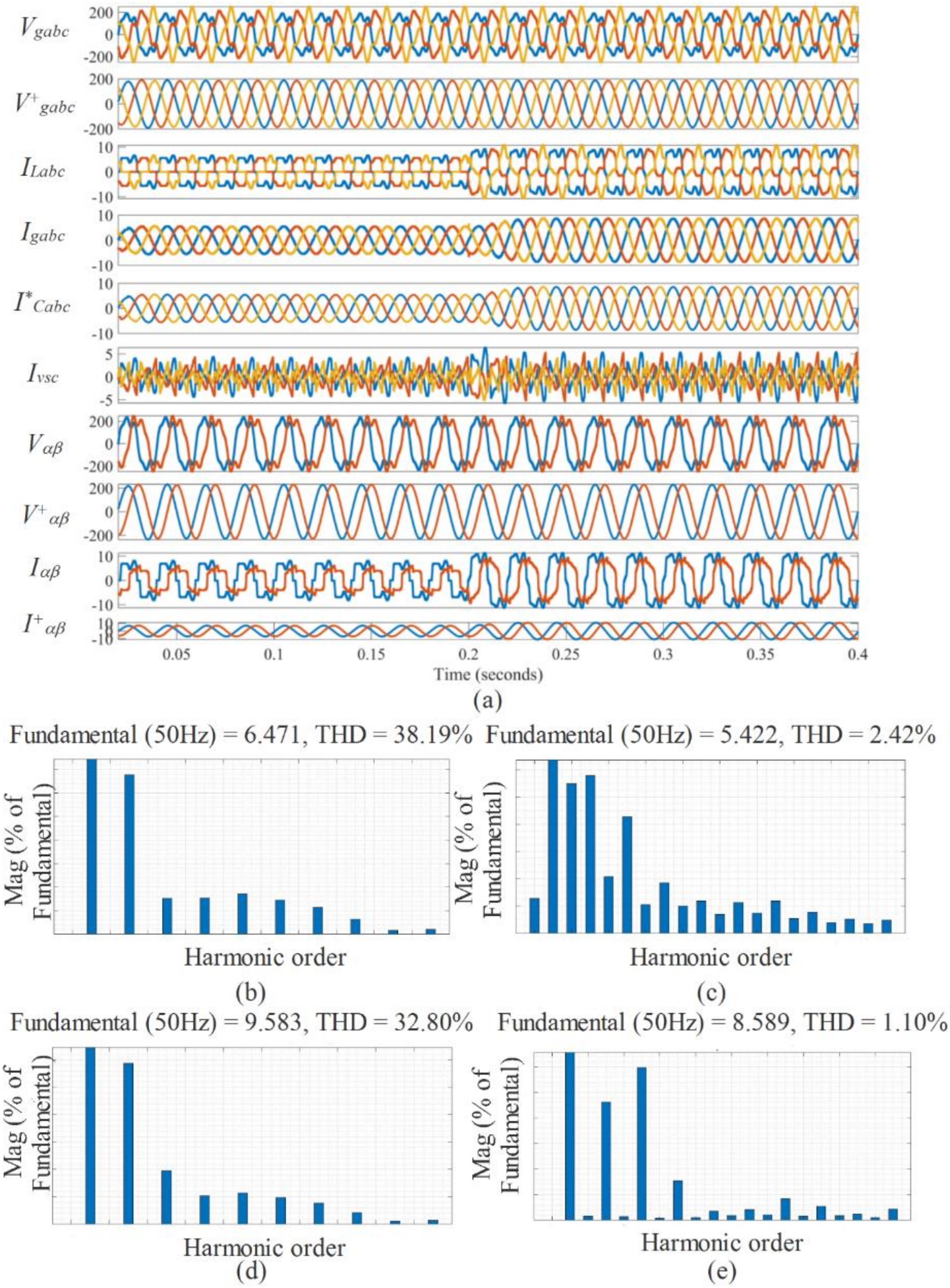

Figure 11 Results under grid voltage with harmonics condition, (a) Simulation, (b) FFT for NLL without controller, (c) FFT for NLL with controller, (d) FFT for both LL and NLL without controller, (e) FFT for both LL and NLL with controller

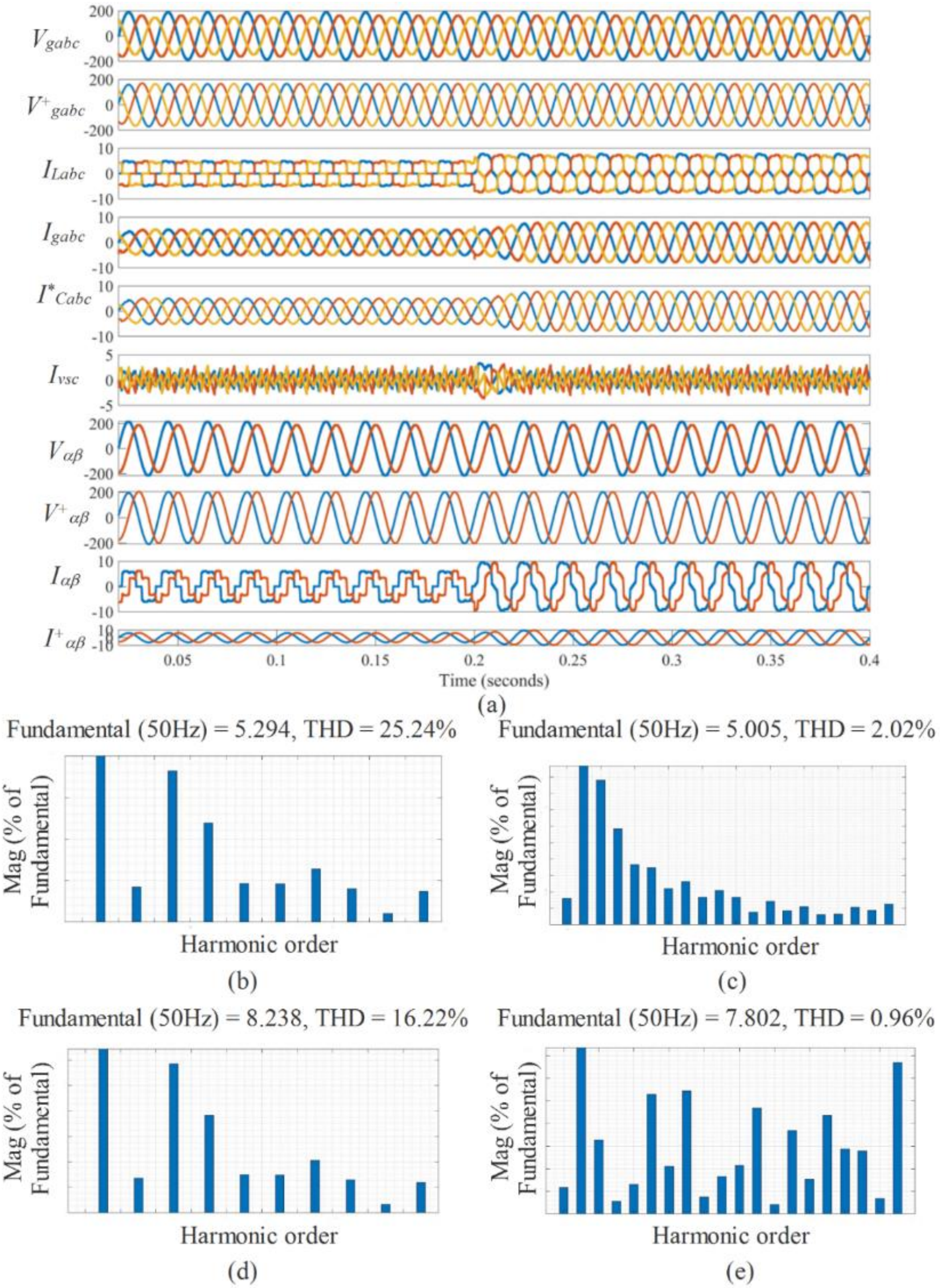

Figure 12 Results under unbalanced grid voltage condition (a) Simulation, (b) FFT for NLL without controller, (c) FFT for NLL with controller, (d) FFT for both LL and NLL without controller, (e) FFT for both LL and NLL with controller

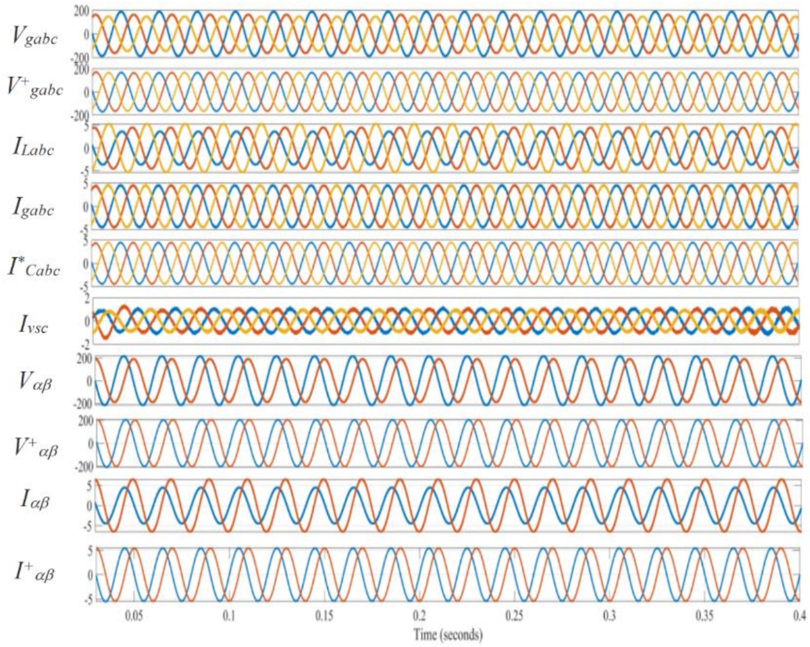

Figure 13 Simulation result unbalance grid voltage condition with unbalanced load

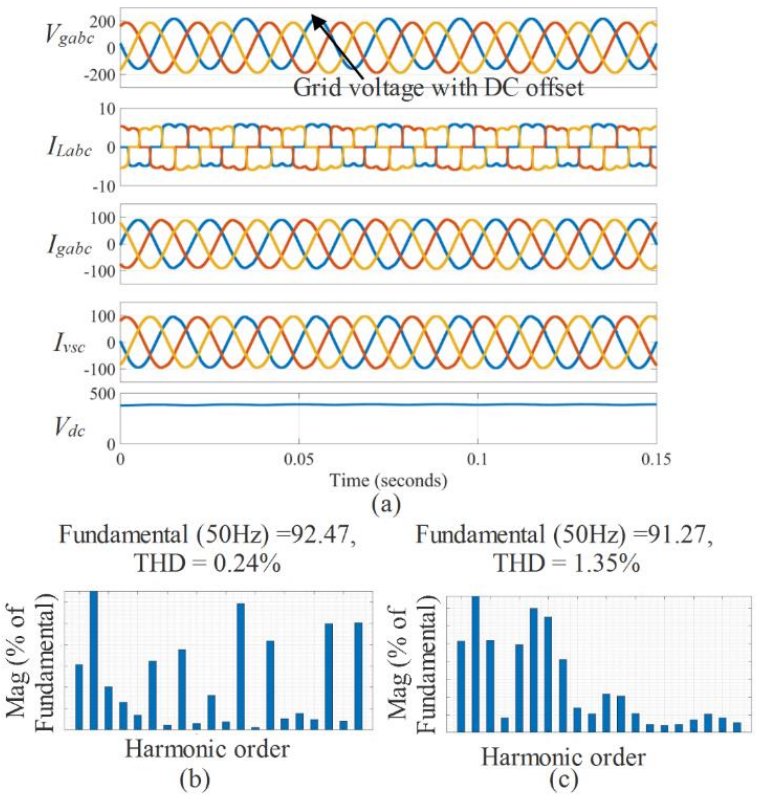

Figure 14 Results under grid voltage with DC offset condition, (a) Simulation, (b) FFT for healthy grid with controller, (c) FFT for DC offset with controller

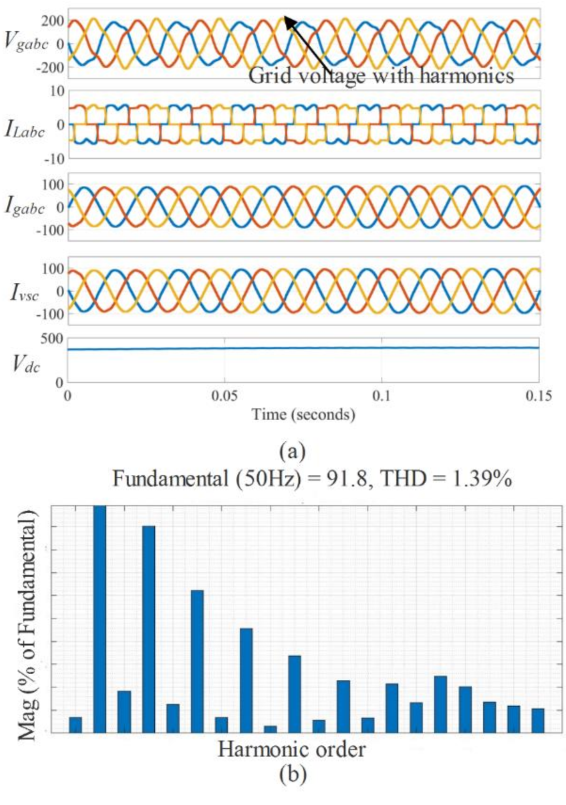

Figure 15 Results under grid voltage with harmonics condition, (a) Simulation, (b) FFT with controller

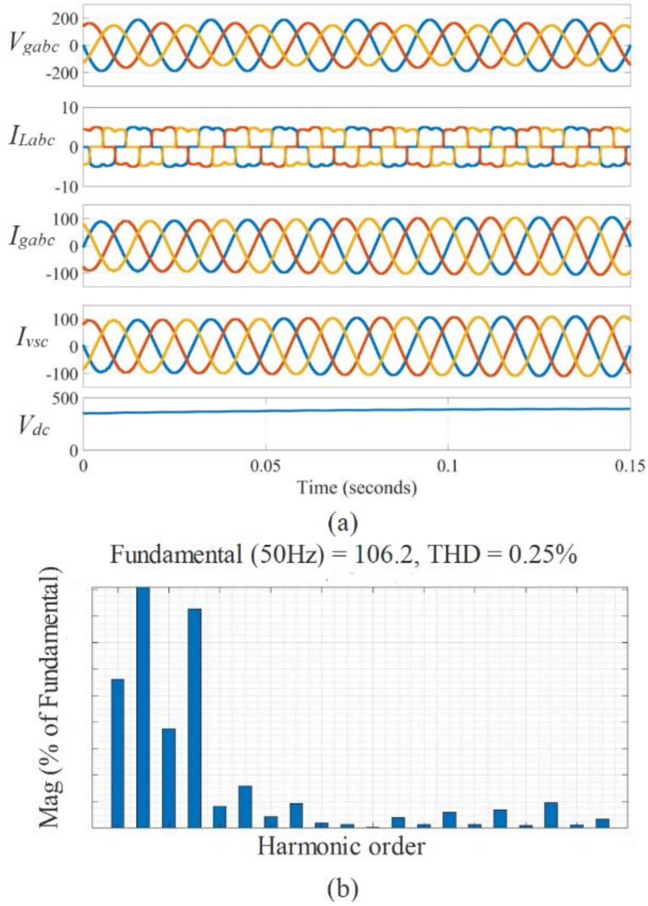

Figure 16 Results under unbalanced grid voltage condition (a) Simulation, (b) FFT with controller

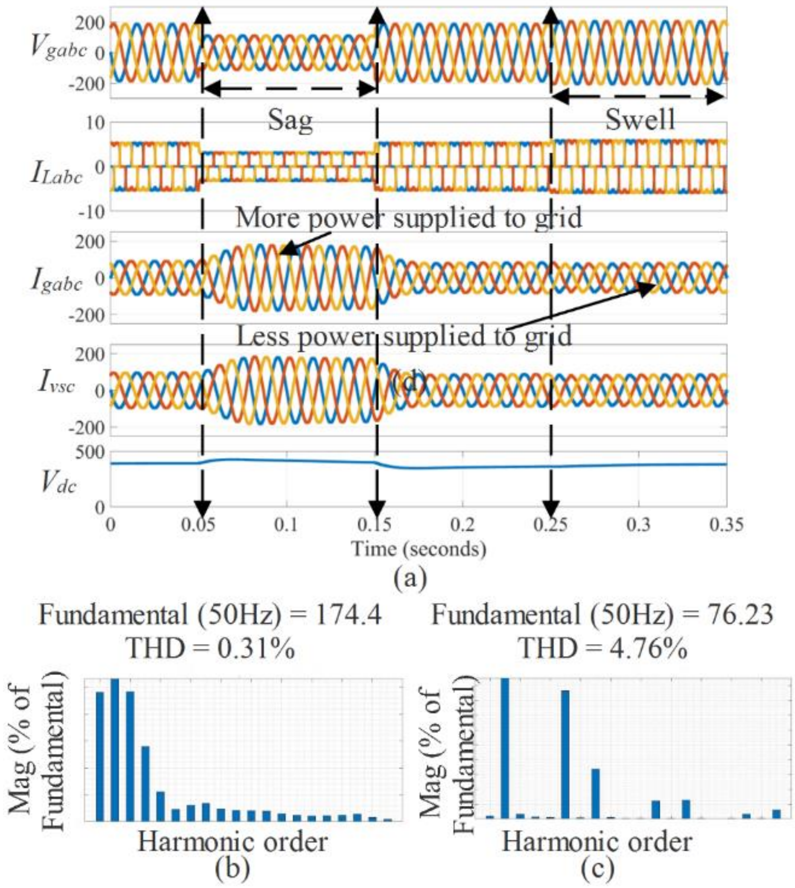

Figure 17 Results under sag and swell condition (a) Simulation, (b) FFT for sag, (c) FFT for swell

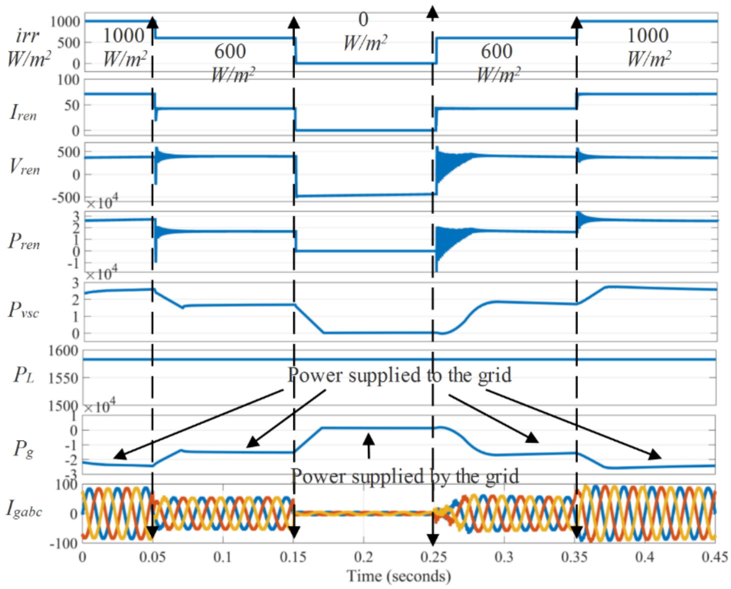

Figure 18 Simulation under variable solar irradiance condition

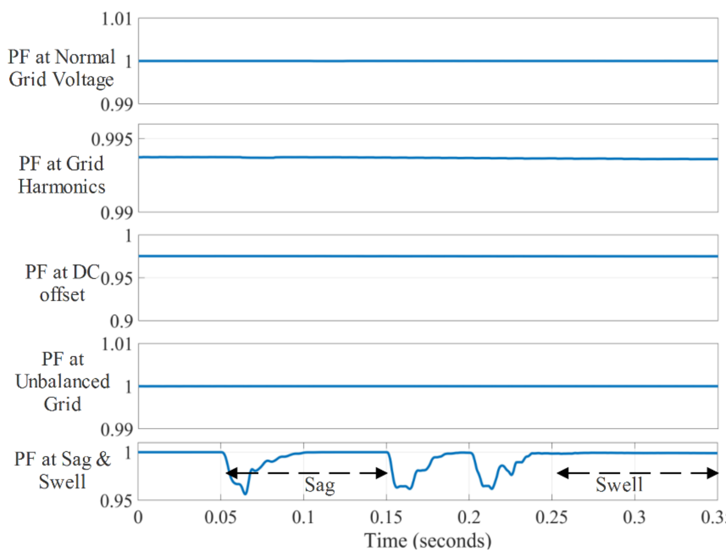

Figure 19 Power factor under various grid voltage condition

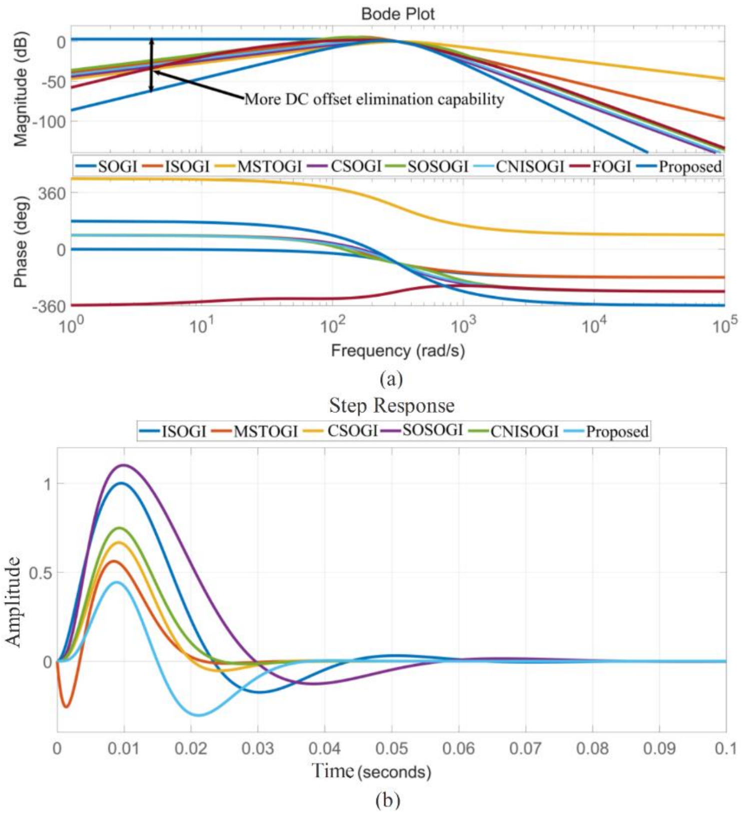

Figure 20 Comparative curve for quadrature axis transfer function, (a) Bode plot, (b) Step response

Table: -

Table-1 Abbreviations and its full form

Abbreviations	Full Form
MPPT	Maximum Power Point Tracking
SiOGI	Sixth Order Generalized Integrator
FLL	Frequency Lock Loop
VSC	Voltage Source Converter
RESs	Renewable Energy Sources
PV	Photovoltaic
PQ	Power Quality
GI	Generalized Integrator
PSCs	Positive Sequence Component
UVT	Unit Vector Template
IRPT	Instantaneous Reactive Power Theory
SRF	Synchronous Reference Frame
ADALINE	ADAptive LInear NEuron
NN	Neural Network
KF	Kalman Filter
DFT	Discrete Fourier Transform
SOGI	Second Order Generalized Integrator

ISOGI	Improved Second Order Generalized Integrator
MSTOGI	Mixed Second Third Order Generalized Integrator
CSOGI	Cascaded Second Order Generalized Integrator
SO-SOGI	Second Order Second Order Generalized Integrator
CNISOGI	Cascaded Non-Identical Second Order Generalized Integrator
FOGI	Fifth Order Generalized Integrator
MSOGI	Multilayer Second Order Generalized Integrator
ROGI	Reduced Order Generalized Integrator
MROGI	Modified Reduced Order Generalized Integrator
V_{dc}	DC Link voltage
V_{dc}^{*}	Reference DC Link Voltage
V_{LL}	Line to Line Voltage
V_{gabc}	Three Phase Grid Voltage
I_{gabc}	Three Phase Grid Current
V_{gabc}^{+}	Positive Sequence Three Phase Grid Voltage
$V_{\alpha\beta}$	$\alpha\beta$ Component of Grid Voltage
$V_{\alpha\beta}^{+}$	Positive Sequence αβ Component of Grid Voltage
V'_{α}, V'_{β}	In Phase $\alpha\beta$ Component of Grid Voltage
qV'_{α}, qV'_{β}	Quadrature $\alpha\beta$ Component of Grid Voltage
V_{tg}	Magnitude of PSCs of grid voltages
I_{Labc}	Three Phase Load Current
I_{Labc}^{+}	Positive Sequence Three Phase Load Current
$I_{\alpha\beta}$	$\alpha\beta$ Component of Load Current
$I_{\alpha\beta}^{+}$	Positive Sequence $\alpha\beta$ Component of Load Current
I'_{α}, I'_{β}	In Phase $\alpha\beta$ Component of Load Current
qI'_{α}, qI'_{β}	Quadrature $\alpha\beta$ Component of Load Current
u_{gpabc}^{+}	Three phases In Phase Unit Vector Template
u_{gqabc}^{+}	Three Phase Quadrature Unit Vector Template
I_a, I_b, I_c	Active Power Component of Load Current
I_{eq}	Average Active Power Component of Load Current
I_{renff}	Renewable Energy Feed-Forward Current
I_{loss}	Loss Component of Converter Current
I_{net}	Total or Net Current
I_{Cabc}^{*}	Three Phase Reference Current
I_{vsc}	VSC Output Current
irr	Solar Irradiance
I_{ren}	Renewable Energy Source Current
V_{ren}	Renewable Energy Source Voltage

P_{ren}	Renewable Energy Source Power
P_{vsc}	VSC Output Power
P_L	Three Phase Load Power
P_g	Three Phase Grid Power
PF	Power Factor
f	Supply Frequence
ω	Supply Angular Frequency
ω'	Corner/Resonance Angular Frequency
Z_L	Line Impedance
L_f	Interfacing Inductor
C_{dc}	DC Bus Capacitor
θ	Phase Angle in Radian
V_{dcoff}	DC Offset Voltage
PI	Proportional and Integral
K_p	PI Controller Proportional Gain
K_i	PI Controller Integral Gain
ξ_1, ξ_2, ξ_3	Damping Factor
K_1, K_2, K_3	Controller Gain
λ	FLL Gain
m	Modulation Index
LL	Linear Load
NLL	Non-Linear Load
UBL	UnBalanced Load
FFT	Fast Fourier Transform
THD	Total Harmonics Distortion
QSG	Quadrature Signal Generator
FC	Fundamental Component
GMD	GeoMagnetic Disturbances
HVDC	High Voltage Direct Current

Table 2 Specification of the system

Specification	**Simulation Value**
V_{gabc}	$230V$
f	$50Hz$
Z_L	$R = 0.01,\ L = 1.5mH$
L_f	$2.2\ mH$
NLL	$R = 60\Omega,\ L = 10mH$
LL per phase	$R = 60\Omega$
C_{dc}	$2200\mu F$
V_{dc}	$375V$

Controller parameter	$K_1 = 1.452$, $K_2 = 1.6$, $K_3 = 2$, $\lambda = -1$
ω	314 rad/sec

Table 3 Comparative analysis

Controller	**SOGI [22]**	**ISOGI [25]**	**MSTOGI [29]**	**CSOGI [31]**	**SOSOGI [32]**	**CNISOGI [33]**	**FOGI [35]**	**Proposed**
Filter types	Advance	Advance	Advance	Advance	Advance	Advance	Advance	Advance
Oscillation	More	Less	More	Less	More	Less	Less	Less
Amplitude tracking	Poor	Better	Better	Low	Better	Better	Better	Better
Frequency tracking	Poor	Better	Better	Low	Better	Better	Better	Better
Phase tracking	Poor	Better	Better	Low	Better	Better	Better	Better
Fundamental component tracking	Poor	Good	Good	Low	Good	Good	Good	Good
Grid synchronisation	Yes	Yes	Yes	Yes	Yes	Yes	Yes	Yes
Accuracy	Less	Medium	Less	Less	Medium	Medium	Medium	High
DC offset elimination	No	Good	Medium	High	High	High	High	Very High
THD by grid harmonics (3rd and 5th harmonics)	3.18%	3.18%	4.16%	3.19%	3.45%	1.98%	3.76%	1.60%
THD by DC offset (50V)	8.91%	1.86%	3.14%	3.31%	1.76%	1.7%	1.65%	1.43%
THD by both grid harmonics and DC offset	10.57%	3.35%	6.20%	4.41%	3.61%	1.97%	4.02%	1.77%
Overshoot	Present	Not present	Not present	Present	Present	Present	Present	Not present
Sampling time	5 μs	5 μs	5 μs	5 μs	5 μs	5 μs	5 μs	5 μs
Static error	More	Less	More	Medium	Medium	Less	Medium	Very less
Settling time	0.04s	0.08s	0.045s	0.06s	0.085s	0.055s	0.1s	0.037s

Table 4 Comparative analysis with conventional controller

Controller	**IRPT [6]**	**SRF [7]**	**Fryze [8]**	**ADALINE [9]**	**Proposed**

Filter types	Conventional	Conventional	Conventional	Conventional	Advance
Voltage fluctuation	Present	Present	Present	Present	Not Present
Harmonics mitigation	Average	Average	Average	Average	Good
Frequency deviations	Present	Present	Present	Present	Good
Power factor	Poor	Poor	Poor	Medium	Good
Unbalancing in grid voltage	Present	Present	Present	Present	Not Present
Accuracy	Less	Less	Less	Medium	High
DC offset elimination	No	No	No	No	Very High
Flicker	Present	Present	Present	Present	Not Present
Current harmonics under voltage Sag	High	High	High	Medium	Low
Current harmonics under voltage Swell	High	High	High	High	Medium
PLL requirements	No	Required	Required	Required	Required
Both current and voltage harmonics mitigation	Not possible	Not possible	Not possible	Not possible	possible
FC extraction	Not possible	Not possible	Not possible	Not possible	possible

Biographies

Priyank Nema is currently a PhD scholar in the School of Electrical and Electronics Engineering at VIT Bhopal University, Sehore, India. His research focuses on addressing power quality issues in grid-connected solar photovoltaic (PV) systems, a critical area in the advancement of renewable energy integration into the power grid. He completed his Bachelor of Engineering (BE) degree in Electrical and Electronics Engineering in 2010 from the University Institute of Technology, Rajiv Gandhi Proudyogiki Vishwavidyalaya (UIT-RGPV), Bhopal. He then pursued a Master of Technology (M.Tech) degree, graduating in 2012 from the Maulana Azad National Institute of Technology (MANIT), Bhopal, where he further developed his expertise in electrical engineering. With a strong academic foundation and a specialized focus on power quality and renewable energy, he is actively contributing to the research community through his investigations into the challenges and solutions related to power quality in solar PV systems connected to the grid. His work aims to enhance the stability, reliability, and efficiency of renewable energy sources in modern power systems.

Sivasankaran Velayutham is a Senior Assistant Professor in School of Electrical and Electronics Engineering at VIT Bhopal University, Sehore India. And has more than 15 years of teaching and research experience; he completed his B.E with specialization in ECE and M.E with specialization of Applied Electronics and Doctorate in the faculty of Information and Communication Engineering. He obtained All UG, PG and PhD from Anna University Chennai. India. He has published 22 papers in peer reviewed international journals and in IEEE international conferences. He also published book chapters and three patents to his credit. He has is reviewer for various reputed international journal. His research interest is in the areas of control systems, IoT based systems design, Heterogenous wireless networks He had been as session chair for various international conferences across the country also he invited as guest speaker at various seminars and workshops.

Narendra Babu P received the Ph.D. and MTech degrees in electrical engineering department with power and energy systems specialization from the National Institute of Technology Meghalaya, Shillong, in 2017and 2022, respectively. He received the B.Tech. degree in electrical and electronics engineering from Jawaharlal Nehru Technological University Hyderabad, Hyderabad, India. Presently, he is working as an Assistant professor at the school of EEE, VIT Bhopal University since 2021. He has as a research experience of 4 years as a Senior Research Fellow/Project Associate with RECTPCL-CSR Funded Project during 2017-2021, Department of Electrical Engineering, National Institute of Technology Meghalaya. He has as an industry experience of 5 years as an assistant electrical engineer during 2010-2015. He has published more than 30 research publications in IEEE Transactions/Journals, international conferences and book chapters. He is a reviewer of several IEEE Transactions, IET, Wiley, Taylor & Francis and other SCI Journals. He is working as an associate editor in several journals. His current research interests include renewable energy technologies, hybrid ac–dc Microgrid, power quality, adaptive control, Solar PV system, power management, and control of grid-tied inverters.